Selective Plane Illumination Microscopy Using Non-Spreading Airy Beams

Aleksandrs Leitis

Supervisor: Johan Axelsson

Co-supervisor: Stefan Andersson-Engels

60 ECTS Master Thesis

Atomic Physics Division

Lund University

May, 2016

Abstract

Recently a new field of microscopy has emerged, known as selective plane illumination microscopy ($SPIM$). Using a $SPIM$ setup the sample is illuminated with a thin light sheet from the side. The selective plane illumination overcomes many problems that conventional microscopes have. Conventional microscopes illuminate the sample axially and collects the light only from the focal plane of the microscope objective. Therefore parts of the sample which are out of focus are illuminated unnecessarily, leading to rapid fluorophore photobleaching and decrease of signal to noise ratio due to out of focus light. The $SPIM$ method overcomes these problems, because only the fluorophores in the focal plane of the objective are excited. Another problem with conventional microscopes is that they are capable of only two-dimensional imaging. The exception are confocal microscopes, but these microscopes are slow and the field of view is restricted to few hundred micrometers. The $SPIM$ method significantly improves the three-dimensional imaging speed and can reach up to few hundred frames per second. This imaging speed enhancement is achieved, because the whole plane is captured with a single snapshot, instead of point by point scanning as in confocal microscopes.

To take all the advantages of the $SPIM$ method it is crucial to form a thin light sheet that extends for the whole field of view. Commercially available lasers have Gaussian beam. It is well known that tightly focused Gaussian beams spread out quickly, therefore there will be good axial resolution only in the central part of the image. Because of that the field of view will be restricted to the Rayleigh range of the Gaussian beam. In this work we present how to create non-spreading Airy beams using only two additional lens elements and how they can be implemented in the $SPIM$ setup to significantly extend the field of view keeping high axial resolution. This is an important advancement since Airy beams would allow larger sized objects, e.g. optically cleared tissue specimens, to be imaged with high resolution. This thesis shows a novel design of a light sheet microscope that opens up new possibilities for biological and medical research.

Popular Science

The field of optical microscopy emerged in late 17th century, when famous Dutch draper and scientist Anton van Leeuwenhoek pioneered the techniques of microscopy. Since then the field has expanded and has greatly influenced the development of biology, chemistry, physics and medical research areas. Recently optical microscopy reached the realms of super resolution and nano scale, therefore allowing to see even single molecules. For this invention in 2014 three scientists were awarded with Nobel prize in chemistry [1]. Overall, four Nobel prizes have been awarded for discoveries and inventions in microscopy. Most of the research in optical microscopy is done to increase the spatial resolution, neglecting the resolution in time. But obviously there are fast biological processes and understanding them would give significant contribution to medicine and biology.

In the last decade a new field of microscopy emerged, called selective plane illumination microscopy (SPIM). What distinguishes SPIM from conventional microscopes is that the sample is illuminated with a thin laser sheet. Therefore fluorescent light will be emitted only from the plane where the light sheet lies. And the light sheet can be made as thin as one hundredth of a human hair width. Therefore the SPIM method allows to image large samples with high temporal resolution and high spatial resolution in all 3 dimensions. With this new technique it is possible to reach up to few thousand frames per second, and it is possible to follow neuron signal propagation in real time. It is a great step forwards for research in neurology. Not only for studying cellular interactions, but also neuronal network interactions throughout the body of small animals. Furthermore bigger and older sample imaging could give better understanding of the neurological diseases that come with age, for instance Alzheimer's disease.

Besides significant increase in temporal resolution, with the SPIM technique it is possible to follow biological processes for much longer time periods compared to conventional microscopes. One can follow the evolution from larvae to fully grown organisms with single cell resolution or biological processes in cells for several days. Therefore it is now possible to follow how diseases evolve in tissue and how well the drugs can affect a disease. Thus it is possible to monitor the disease and the treatment in all stages. This is a significant improvement compared to conventional microscopes: now it is possible to study diseases and drug efficacy like never before.

List of symbols and abbreviations

AO — Airy Optics

BE — Beam Expander

BS — Beam Splitter

CL — Collimation Lens

CM — Confocal Microscope

DSLS — Digitally Scanned Light Sheet

FL — Focusing Lens

FM — Fluorescence Microscopy

FOV — Field of View

FP — Focal Plane

FWHM — Full Width Half Maximum

GM — Galvo Mirror

NA — Numerical Aperture

OTF — Optical Transfer Function

PSF — Point Spread Function

SL — Scan Lens

SNR — Signal to Noise Ratio

SPIM — Selective Plane Illumination Microscopy

List of Figures

Contents

1 Introduction

1.1 Fluorescence

Fluorescence is a well known process, and almost everyone has seen fluorescent light either in nature (firefly) or from artificial objects (fluorescent light bulbs). The most common fluorescent mechanisms are photoluminescence (after electromagnetic radiation absorption), chemiluminescence (after chemical reactions) and electroluminescence (caused by electric current). In this work we will focus on the fluorescence process that is caused by electromagnetic radiation absorption.

To describe the photoluminiscence we have to characterize energy levels of a molecule. Lets take a look at a simple molecule that consists of two atoms. From quantum mechanics, it follows that an electron in an electric potential has bound states with discrete energies, called electronic states [2]. The energy difference of electronic states is around 1-5 eV which correspond to UV and visible spectrum [3].

These two atoms in a molecule can also vibrate. This motion can be approximated as a harmonic oscillator. Therefore the potential energy is an

$$V = kr^2, \tag{1}$$

where k is the spring constant and r is the distance between atom nuclei. Solving the Schrödinger wave equation, for a particle in a harmonic potential gives a discrete energy spectrum, where all the energy levels are equidistant. In reality the potential is not a symmetric quadratic function, and is better described as the Morse potential, see figure 1.1. As a consequence of the anharmonic Morse potential the energy levels are not equidistant any more, see figure 1.1. The energy separation of two vibration levels is approximately 0.1 eV which corresponds to infrared spectrum.

Besides electronic and vibrational movement, molecules can also rotate, therefore they will have also rotational energy. For a rigid diatomic molecule the rotational energy is obtained from the Schrödinger equation with the Hamiltonian expressed as an angular momentum operator [3].

$$\hat{H}_{rot}\Psi = \frac{\hat{L}^2}{2I}\Psi = E_{rot}\Psi, \tag{2}$$

where Ψ is the wave function, E_{rot} is the rotation energy, $\hat{L}$ and is the angular momentum

operator and $\hat{H}_{rot}$ is the Hamiltonian. The solution of equation 2 gives discrete energy spectrum with energies E=J(J+1)B, where J is the rotation quantum number and B is the rotation constant. The rotation energy is approximately 10^{-4} eV therefore rotation transitions are visible in the microwave region. The rotation energy levels are not shown in the figure 1.1, because they are 3 orders of magnitude smaller than the vibration energy levels.

When the energy levels are characterized, we can describe the Photoluminiscence process. This process starts with the excitation of light photon absorption, see figure 1.1. To excite the molecule the photon has to match the energy difference between the ground state and excited state, and the angular momentum conservation law has also to be satisfied. Therefore not all of the transitions are allowed. The selection rules show which transitions have high probability and which transitions have low probability. Besides the selection rules, the transition probability will be governed also by the Franck-Condon principle.

After the absorption process, the outer electron of the molecule is excited to higher rovibrational states in an excited electronic state. Then, to satisfy the Stefan-Boltzman distribution, the electron relaxes to a lower vibrational state. This relaxation process is radiationless, the energy is dissipated as kinetic energy to the same molecule or surrounding molecules. Then the electron relaxes to the ground electronic state and emits a photon [4, 5]. Because the electron has lost some energy from relaxation in the exited state, the fluorescence light is with lower energy. Also the electron relaxes to some higher vibrational states in the ground electronic state, see figure 1.1, therefore the fluorescence emission covers longer wavelength spectrum compared to excitation light, see figure 1.1.

The fluorescence process has been proven to be very useful in microscopy. The great advantage is that the fluorescent light can be filtered out of excitation light. Another advantage is that fluorescent molecules can be synthesized to bind to specific biological molecules. Therefore this technique allows to labelling of e.g. cells, membranes, organelles, enzymes, nuclei of cells and drugs. By using fluorescence microscopes (FM) it is possible to study one particular biological process. Therefore FM is a remarkable tool for research in biology, medicine and pharmacology. Unfortunately only few biological specimen have strong endogenous fluorophores, therefore most of biological specimen have to be stained with fluorophores. Some samples can be genetically modified to make their proteins fluorescent, for example zebrafish and mice [6, 7, 8].

There are some limitations to the use of fluorescence. For example, fluorophores tend to bleach due to irreversible damage induced by the excitation light. The process of repeated electron excitation in the molecule eventually ruptures the chemical bond. After this chemical damage, the molecule is not fluorescent any more. Therefore the sample observation time is limited. The photobleaching rate can be reduced by using more stable fluorescent molecules or by reduced illumination intensity.

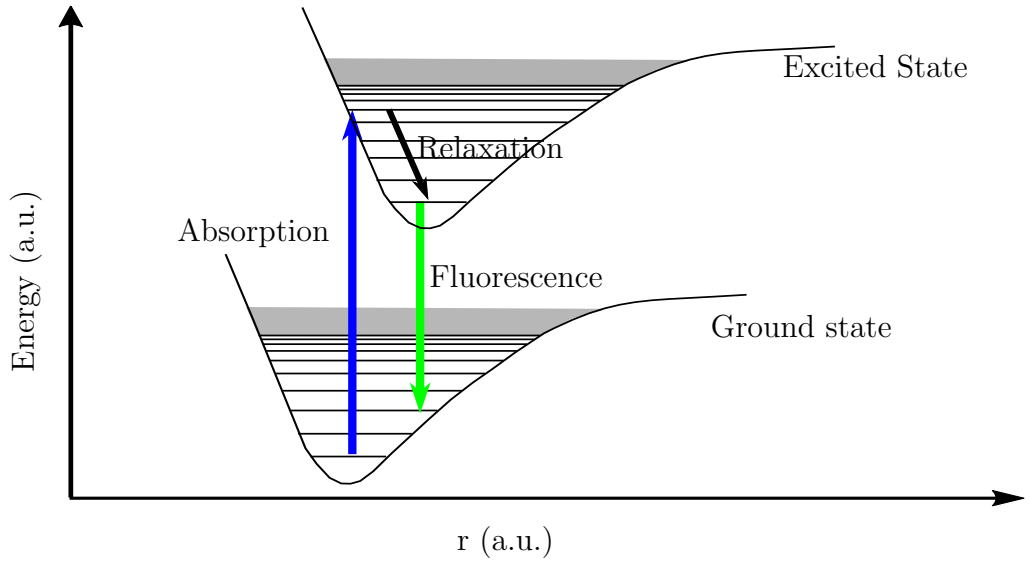

Figure 1.1: Fluorescence energy diagram, where blue arrow shows absorption, black arrow relaxation, and green arrow fluorescence. R is the distance between atoms in a molecule.

.

1.2 Fluorescence Microscopy

The fluorescence microscope (FM) is a microscope that uses fluorescence emission light to create an image. There exists several FM methods, like the wide field fluorescence microscopy, confocal microscopy (CM), selective plane illumination microscopy and multiphoton microscopy. One major advancement within the field of fluorescence microscopy was the invention of the laser scanning confocal microscope. The first confocal microscope that was able to create three dimensional images was created in 1969 by M. David Egger and Paul Davidovits [9]. Nowadays the CM has become the most common tool for live cell 3D imaging. Using high numerical aperture (NA) objectives the light is tightly focused to one small spot, therefore the strongest fluorescence signal will be from this focal point. Nevertheless light propagates through the sample and excites fluorophores also outside the focal spot. To reduce the background fluorescence a pinhole is placed in front of the camera, that only allows light from the focal point to get through. This setup significantly increases the signal to noise ratio, gives high contrast and diffraction limited resolution [10]. In CM the image is formed through point by point scanning. Either the light focal point is moved or the sample itself is moved through the focal spot. The cost of the high resolution is that this imaging technique is slow therefore it is not possible to follow fast biological processes. Moreover confocal microscopes have high phototoxicity, due to the point-by-point scanning, leading to unnecessary illumination with out-of-focus light. This out of focus light increases the fluorophore photo-bleaching rate, therefore it is not possible to follow biological processes for long time periods. To have good axial resolution,

confocal microscopes require high numerical aperture objectives. And high NA restricts the field of view. Therefore there is a trade off between the resolution and the field of view. The maximum field of view of confocal microscopes is around 500 micrometers.

1.3 Selective Plane Illumination Microscopy

Recently a new microscopy technique was introduced, given the name selective plane illumination microscopy (SPIM). Although a very active research field today, the predecessor to SPIM was introduced in the early 1900s [11, 12, 13]. In 1903 H.F.W. Siedentopf and R.A. Zsigmondy invented the first selective plane illumination microscope. The 1925 Nobel Prize in Chemistry was awarded to R. Zsigmondy for his demonstration of the heterogeneous nature of colloid solutions and for the methods he used [14].

In the SPIM setup the sample is illuminated from the side with a thin light sheet. Therefore the fluorescence light will be emitted only from the plane where the excitation light sheet lies, see figure 1.2. Using laser radiation it is possible to form light sheets that are considerably thinner than the objective depth of focus. Also it is easy to place this excitation light sheet in the focal plane of the detection objective. Therefore it is possible to improve the axial resolution of microscopes using selective plane illumination methods $SPIM$.

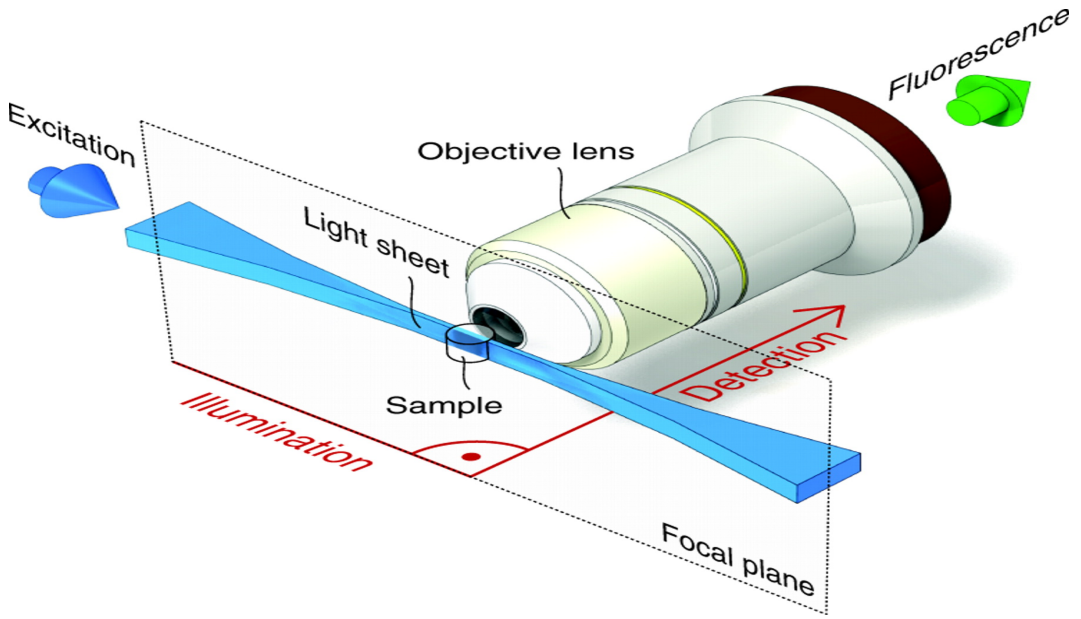

Figure 1.2: Selective plane illumination method [15]

.

The SPIM setup has also other advantages compared to conventional microscopes. The conventional light microscopes focuses the light to a small focal point and illuminates all the sample, but the SPIM microscope illuminates only the plane which is in the focus of the microscope objective. Therefore the biological specimen is illuminated

much more efficiently, and parts of the specimen which are out of focal plane are not unnecessary illuminated. Thus the SPIM method reduces the photobleaching of the fluorescent molecules [16, 17]. Therefore it is possible to follow biological processes for longer periods of time. Furthermore the illumination from the side significantly reduces the out of focus light therefore greatly increasing the signal to noise ratio. Another advantage of the SPIM setup is much higher speed of 3D image acquisition [18]. Conventional confocal microscopes illuminate one spot at the time and the image is constructed by scanning each point in the focal plane. But, as stated before, the SPIM microscope illuminates the whole focal plane, while the fluorescence is detected by a sCMOS camera. Therefore the imaging speed is much higher compared to confocal microscopes. To construct a 3D image using a$SPIM$ microscope either the sample or the light sheet is translated along the detection axis. The increased imaging speed allows to follow fast biological processes, for instance neuron signal propagation or heartbeats of zebrafish [19, 20].

New techniques of biological sample preparation have allowed to make up to few cm big samples almost transparent. It is done by optical clearing process. The sample is put in several clearing agents that make the tissue and cell medium fit the refractive index of cell membranes. Therefore light passing through the sample is not refracted and reflected any more. Thus the scattering coefficient is significantly reduced and light passes straight through the sample. The optical clearing process minimally affects the fluorophore distribution, therefore using SPIM microscope it is possible to image large optically cleared samples with microscopic resolution in all three dimensions [21]. This new field of microscopy is called Ultramicroscopy [22, 23].

The limitations of the SPIM method is that the laser sheet is not uniform along the propagation axis. To form the light sheet usually lasers with Gaussian beam profile are used. However tightly focused Gaussian beams spread out quickly, therefore there will be good axial resolution only in the central part of the image. Because of this, the field of view will be restricted to the Rayleigh range of the Gaussian beam. This work is dedicated to overcome this problem. In the 1978 N.L. Balazs and M.V. Berry showed that there exists wave packets known as Airy beams that do not spread out [24]. In 2007 the first light beam with Airy profile was created [25]. These beams maintain their width of the beam waist for more than 10 times longer distances compared to Gaussian beams[26, 27]. Therefore by implementing Airy beams in the SPIM setup it is possible to extend the field of view maintaining the same axial resolution.

1.4 Purpose and Aims

The aims of this thesis are summarized in the following bullet list.

- Make an optical design for light sheet formation, to image large objects, with homogeneous laser sheet intensity throughout the field of view.

- Make computer simulations with 2 cylindrical lenses for Airy beam generation and find an optimal setup.
- Build the designed light sheet microscope with Gaussian and Airy optics.
- Compare the simulations of Airy beams and real measurements.
- Implement approaches for deconvolution of the three dimensional microscopy datasets.
- Measure and compare the resolution and field of view of Gaussian and Airy beams.

2 Theory

2.1 Light sheet formation

Light sheet formation is a central part of the SPIM microscope that determines the axial resolution. There exists several ways how to form the light sheet. The simplest setup for light sheet formation consists of cylindrical and spherical lenses arranged in a way that the focal planes of both lenses coincide. In such a setup the light sheet will be formed throughout the depth of the second lens focus. The advantage of this setup is simplicity and low cost, but the disadvantage is that the light sheet does not have uniform intensity and using single lens it is not possible to focus a beam very tightly. To create very thin light sheets the spherical lens is replaced with a microscope objective. Using high NA objectives diffraction-limited resolution in all 3 dimensions can be achieved [8]. The drawback of High NA objectives is that the working distance is short, therefore the sample size is limited. In both setups with spherical lens and objective, the light sheet will have heterogeneous intensity. This follows from the characteristics of the laser beam profile. The commercially available laser sources usually have a Gaussian beam profile. From Fourier optics follows that a spherical lens performs spatial Fourier transform on the beam profile [28]. The Fourier transform of a Gaussian function remains Gaussian, thus the light sheet will have a Gaussian intensity profile. Therefore less molecules will be excited at the sides where the intensity is lower, leading to dimmer image sides.

To compensate this heterogeneity in the excitation light profile one can use a slit. In the setup with a slit the beam is expanded and sent through a slit which allows only the middle part of the beam to propagate through. In such a way the light sheet intensity profile is more homogeneous, but it reduces the power of the excitation light and also introduces side lobes due to diffraction.

Another approach to overcome the heterogeneous intensity profile of excitation beam is to use a rotating mirror and a scan lens. At first the beam is reflected from the rotating mirror in different angles. To make the outgoing beams parallel, the rotating mirror is placed in the focal plane of the scan lens. By rotating the mirror the beam will be scanned across the whole field of view giving uniform average excitation intensity profile. This arrangement for light sheet creation is know as digitally scanned light sheet method [29, 30].

It is apparent that every focused beam diverges. As the beam width determines the

axial resolution, the sides of the image will have worse axial resolution than in the center of the image. Therefore to have good and homogeneous axial resolution one has to limit the field of view. One way how to overcome this problem is by using non-diverging beams, like Bessel beams or Airy beams. These beams maintain their width for longer distances, but the disadvantage is that they have side lobes which make the images blurred. The side lobes increase the out of focus light and reduce the signal to noise ratio. Using Airy beams it is possible to compensate the blur with deconvolution algorithms. In the setup with Bessel beams it is possible to significantly reduce the side lobes using two photon absorption processes. The probability to absorb two photons is proportional to the squared intensity. Therefore absorption probability in the main peak is considerably larger than in one photon processes. Therefore two-photon processes in this case results in better resolution and also increased signal to noise ratio [31]. It is also possible to expand the field of view by moving the sample through the light sheet along the beam axis and then merging the images together [32]. The drawback of this method is increased photobleaching, the temporal resolution is reduced, in addition the image stitching process induces artefacts.

2.2 Beam profile

2.2.1 Gaussian beam

Usually the output beam of a laser has Gaussian beam profile. The Fourier transform of a Gaussian function is also a Gaussian function. Therefore the Beam profile at the focal plane of a spherical lens is going to have a Gaussian profile. The beam waist or the minimum beam width can be calculated using the following equation [28].

$$w_0 = \frac{4\pi\lambda}{D}, \tag{3}$$

where λ is the excitation wavelength and D is the beam diameter entering the lens. Of course the beam after the focal plane will spread out. The following Equation shows how quickly the beam spreads out [28].

$$\begin{aligned} w(z) &= w_0\sqrt{1+\left(\frac{z}{z_r^2}\right)^2} \\ z_r &= \frac{\pi w_0^2}{\lambda} \end{aligned} \tag{4}$$

where z_r is depth of focus and it shows at what distance the beam width w has expanded to $\sqrt{2}w_0$. Equation 4 shows that depth of focus z_r is proportional to beam waist w_0 squared. In the light sheet microscope design the depth of focus of the laser

sheet is set to cover the field of view of the microscope. Therefore high axial resolution will lead to small field of view and large field of view will lead to poor axial resolution. This is inevitable due to the Heisenberg's uncertainty principle. The more tightly photons are confined the more quickly they will spread out.

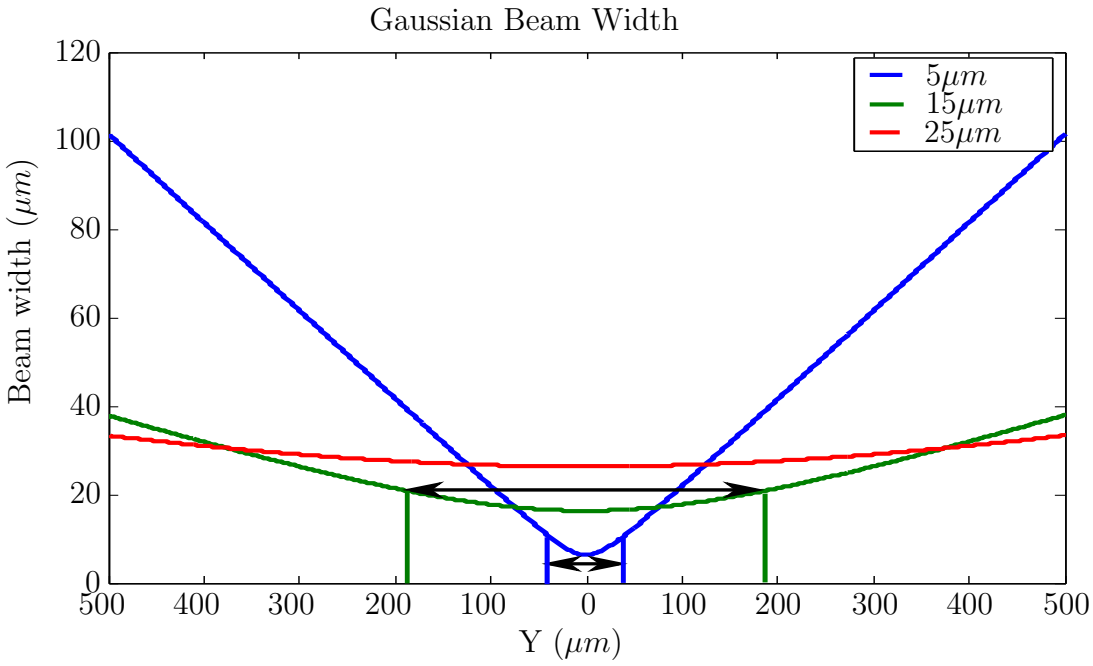

Figure 2.1: Gaussian beam width as a function of propagation distance for different beam waists. Arrows shows the depth of focus.

2.2.2 Bessel beam

To overcome the problem with Gaussian beam intensity spread one can use non-diffracting beams. The first of this kind, called Bessel beams, were originally noted by Durnin [33]. A Bessel beam gets its name from the description of such a beam using a Bessel function, and this leads to a predicted cross-sectional profile of a set of concentric rings. Mathematically, the Bessel beam can contain an infinite number of rings, and so over an infinite area it would carry infinite power. So the conclusion must be that it is not possible to make a Bessel beam [34]. But it is possible to create an approximation of Bessel beam with exponentially decaying side lobes. This means that the beam will be constrained to a finite volume. This confinement will lead to the diffraction, but still the central core of Bessel beams is significantly less divergent compared to Gaussian beams. A disadvantage of Bessel beams is that they have side rings, see figure 2.2. However it is possible to considerably reduce the side lobes by applying two photon absorption processes [35].

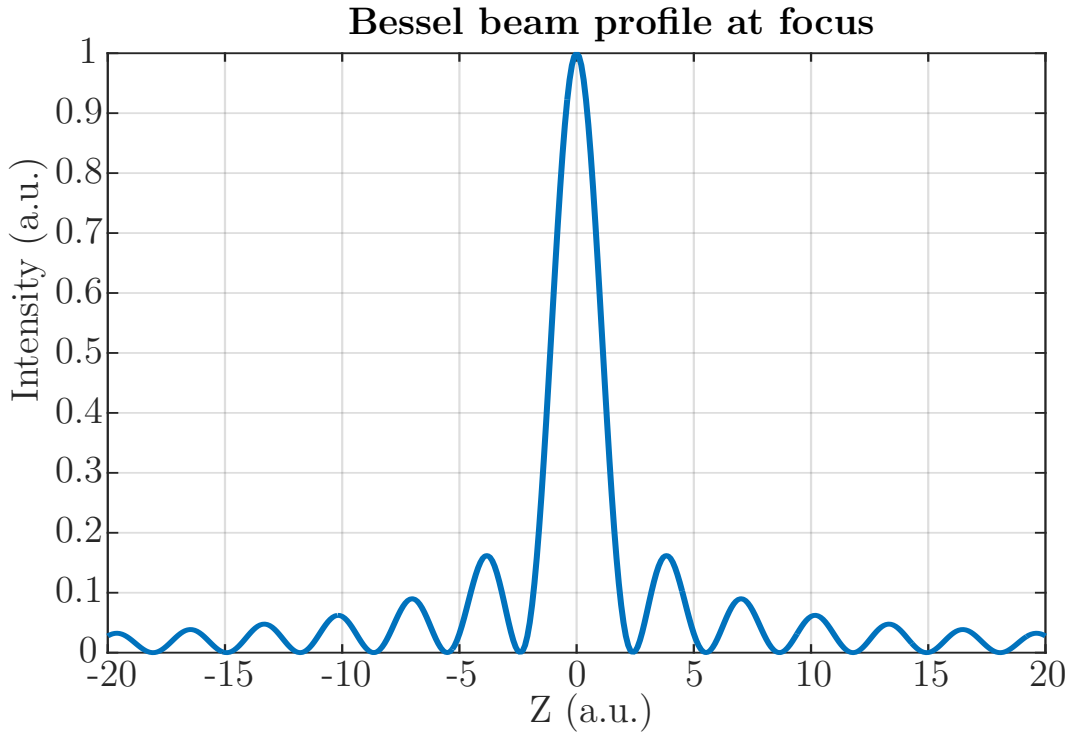

Figure 2.2: Bessel beam profile at focus

2.2.3 Airy beam

Another kind of non-diffracting beams are Airy beams. The Airy function (Ai(x)) is the solution to the simplest second-order linear differential equation 5. This equation is named after British astronomer George Biddell Airy (18011892).

$$\frac{d^2E}{dz^2} - zE = 0, \tag{5}$$

where E is the electric field and z is the spatial coordinate. In 1979 Berry and Balazs theoretically demonstrated that the Schrödinger equation describing a free particle can exhibit a non-spreading Airy wavepacket solution [24]. The Airy beam like the Bessel beam also consists of infinite side lobes covering an infinite area. So it is obvious that in reality it is not possible to generate an Airy beam because it would require infinite energy. Nevertheless, it is possible to generate an approximation of the Airy beam. In this case the electric field can be described as

$$E = Ai(bz)e^{abz}, \tag{6}$$

where a is a positive constant. When z is larger than zero the Airy function decays very quickly to zero. Therefore when $z \to \infty$ then $Ai(bz)e^{abz} \to 0$. To truncate the beam also when $z \to -\infty$ constant a has to be positive. The generation of such Airy beams relies on the fact that the spatial Fourier transform of an exponentially truncated

Airy function is a Gaussian beam modulated with a cubic phase [26, 25, 27, 36]. As stated before a spherical lens at the focal plane creates spatial Fourier transform of the incoming beam. Accordingly an incoming Gaussian beam with cubic phase modulation will appear as an Airy beam at the Focal plane of the lens. The Airy beam ballistics along the propagation axis can be calculated using three equation system below.

$$I(z,y) = \left(Ai(0,\gamma)\cdot e^{\beta}\right)^2 \tag{7a}$$

$$\gamma = bz - \left(\frac{b^2 y}{k}\right)^2 + i\frac{ab^2 y}{k} \tag{7b}$$

$$\beta = abz - \frac{a}{2}\left(\frac{b^2 y}{k}\right)^2 - \frac{i}{12}\left(\frac{b^2 y}{k}\right)^2 + i\frac{a^2 b^2 y}{2k} + i\frac{b^3 zy}{2k}, \tag{7c}$$

where the constant $k = \frac{2\pi}{n\lambda}$ is the wave vector, λ is the excitation wavelength and n is the refractive coefficient. This equation system is derived by solving paraxial beam propagation equation using equation 6 as a boundary condition [25]. From equations 7a,7b,7c it follows that by measuring the beam profile at focus (y=0), one can calculate the decay constant a and the constant b. Using these two values it is possible to simulate the Airy beam ballistics and use this theoretical fit for image deconvolution.

In the figure 2.3 one can see the ballistics of a one dimensional Airy beam and the beam profile at the focus. It is evident that the Beam profile has several peaks and also that the Beam has curvature.

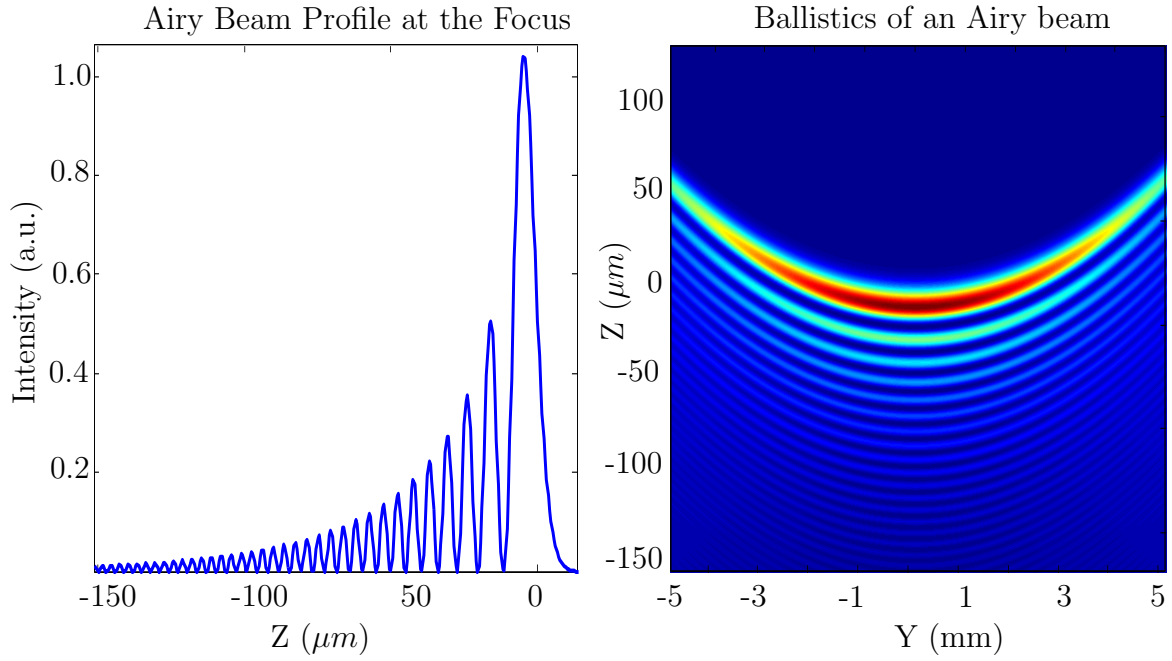

Figure 2.3: 1D Airy beam profile at focal plane

Common practice to induce cubic phase modulation is by using spatial light modulator. But there exists alternatives to this approach of cubic phase modulation. The cubic phase modulation could also be induced by aberrations in tilted and shifted lenses. The simplest approach to create a one dimensional Airy beam is by using a single tilted lens [37]. But in that case the beam must be stationary, therefore one cannot use a single lens to generate an Airy beam generation for SPIM microscopy. The aberrations induced by a lens can be calculated using the Seidel equation [38]:

$$\phi^{(4)} = -\frac{1}{4}B\rho^4 - \frac{1}{2}(2C\cos^2\theta + D)r_0^2\rho^2 + Er_0^3\rho\cos\theta + Fr_0\rho^3\cos\theta, \tag{8}$$

where $\phi^{(4)}$ is phase shift, B is the spherical aberration coefficient, C is the astigmatism coefficient, D is the field curvature coefficient, E is the distortion coefficient, F is the coma aberration coefficient, θ is the polar angle at the exit pupil of the lens, r_0 is the object height and ρ is the zonal radius. From the equation 8 follows that only the terms that contain ρ^3 will induce the cubic phase modulation. From the equation 8 one can see that only the coma aberration term will induce cubic phase modulation. The required cubic phase modulation for Airy beam generation is a one dimensional process, therefore one dimensional elements has to be used [26]. From this follows that cylindrical lenses should be used to induce necessary cubic phase modulation. And in the case of the cylindrical lenses the Seidel equation 8 can be simplified, as follows

$$\phi^{(4)} = -\frac{1}{4}Bx^4 - \frac{1}{2}(2C + D)r_0^2x^2 + Ex_0^3x + Fx_0x^3. \tag{9}$$

Here x is the distance from the lens centre and x_0 is the object height. From equation 9 it is evident that besides the coma aberration term there will be also other terms that wash out the Airy pattern in the focal plane. Using telescopic arrangement with two precisely misaligned lenses it is possible to significantly reduce the other terms and make the cubic phase modulation dominant. It is well know in the field of optical design that aberrations in an optical setup can be minimized using lenses with opposite signs of aberration coefficients [38]. Equation 9 shows that the first lens has to be displaced or either tilted, so the incoming beam would enter the lens at bigger height x_0. The optical setup for Airy beam generation is shown in the figure 2.4.

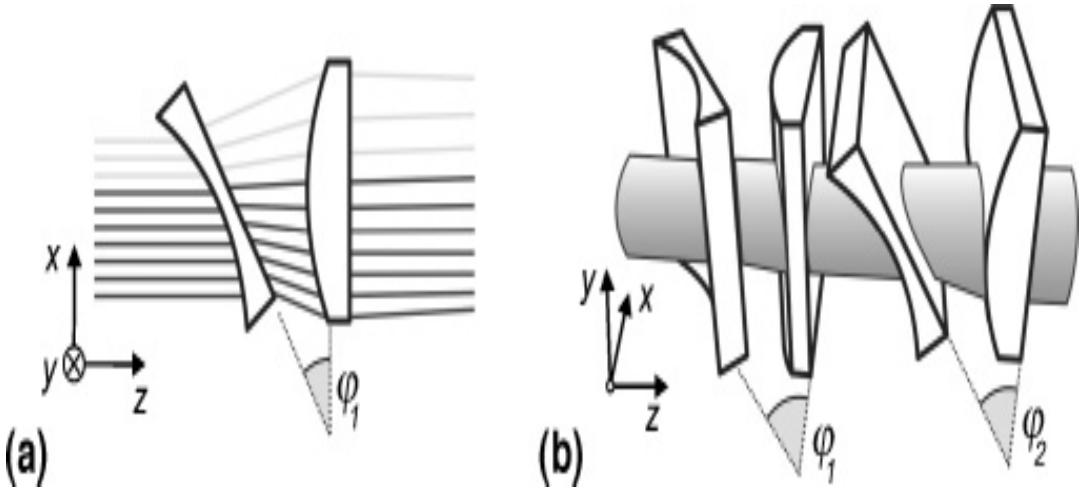

Figure 2.4: (a)Two lens setup for cubic phase modulation and (b) four lens system for 2D cubic phase modulation [26].

2.3 Point Spread Function and Optical Transfer Function

The image never completely reflects the real fluorophore distribution, because: First, fluorophores are much smaller than the diffraction limited resolution. Second, the imaging system has some artefacts from aberrations, lens misalignment, optical filters, etc. The function that characterizes the imaging system's blur and artefacts is called point spread function (PSF). The image can be described as a convolution between real fluorophore distribution and PSF:

$$I(x,y,z) = \int F(x,y,z)PSF(x-x',y-y',z-z')dx'dy'dz', \tag{10}$$

where $I(x,y,z)$ is intensity of the image pixels, $F(x,y,z)$ is the fluorophore distribution, and $PSF(x,y,z)$ is the point spread function. Most of the PSF will have one bright central peak and dim side lobes (Airy disks). As the Airy disks have much lower intensity, the point spread function near the focal plane can be approximated by a Gaussian curve [39]. Usually due to aberrations the lateral resolution in x and y directions are not the same. Nevertheless, asymmetric Gaussian function can be used for image enhancement [40].

The point spread function of the imaging system can be measured using small fluorescent spheres with known diameter that are smaller than the theoretical resolution of the system. [41]. Once the PSF is known it is possible to deconvolve the image and enhance the resolution of the imaging system.

From the convolution theorem follows that in the Fourier space convolution is a

simple multiplication. Therefore in the Fourier space equation 10 would look like

$$\mathcal{F}[I(x,y,z)] = \mathcal{F}[F(x,y,z)] \cdot \mathcal{F}[PSF(x,y,z)], \tag{11}$$

where $\mathcal{F}$ is the Fourier transform operator. The Fourier transform of the point spread function is called optical transfer function (OTF) [42]. OTF shows what range of spatial frequencies the optical system can image. The higher the maximum spatial frequency the better resolution of the microscope.

2.4 Deconvolution for Image Enhancement

The recorded image can be seen as the convolution of the light sheet intensity profile and the fluorophore distribution. Therefore standard deconvolution methods can be used to improve the axial resolution of the 3D image. The simplest way to deconvolve the image would be the calculation of the Fourier transform of the fluorophore distribution:

$$\mathcal{F}[F(x,y,z)] = \frac{\mathcal{F}[I(x,y,z)]}{OTF} \tag{12}$$

In practice, this method does not work well, because it amplifies the noise. Therefore if the noise is high then the deconvolved image will be even more blurred than the original. There exists several deconvolution algorithms, that takes into account the noise. One of the simplest ones is the Wiener deconvolution algorithm:

$$\mathcal{F}[F(x,y,z)] = \mathcal{F}[I(x,y,z)]\frac{OTF}{OTF^2 + \frac{1}{SNR}}, \tag{13}$$

where SNR is signal to noise ratio. From equation 13 it can be seen that the additional term reduces the noise amplification. And when noise reaches zero, then equation 13 becomes the same as equation12. But the Wiener filter has drawbacks. For example small inaccuracies in the OTF will induce large errors in the deconvoluted image. Second, some parts of OTF can be suppressed during the deconvolution, therefore affecting the whole image [41]. Moreover images that are deconvolved with Wiener filter can have negative pixel values, Which is not feasible, since fluorescence has always positive flux.

Besides Wiener filtering there exists more complex deconvolution methods. One of the most commonly used techniques is nonlinear constrained iterative deconvolution algorithm [41]. This method requires higher computer power, but it is possible to correct the blur even without measuring the PSF [43], for instance blind deconvolution method. Nonlinear deconvolution methods never gives out negative pixel values in the deconvolved image. This problem arises in low intensity images that have been deconvolved with linear methods. A full description of the nonlinear deconvolution algorithms is out of the scope of this thesis. Therefore only a brief description of nonlinear deconvolution algorithm is

given in the following part. At first one has to set an initial image for the deconvolution. Then the algorithm starts an iterative loop where new estimates of point spread function and fluorophore distribution are calculated based on the previous ones. Besides, after each step all negative pixel values are set to zero, therefore ensuring that the fluorescence flux is non-negative. After a predefined number of iterations the algorithm gives out deconvolved image.

2.5 Signal to Noise Ratio Enhancement

Almost all biological media scatters light, this property arises from the refractive index difference between cell membranes and the cytoplasm. Therefore part of the light in the laser sheet will be scattered. This scattered light can excite fluorophores outside the focal plane leading to out of focus fluorescent light. Inevitably it will increase background intensity and will reduce SNR. But there exists several methods how to reduce the impact of scattering.

2.5.1 Confocal Slit Arrangement

Similarly to confocal microscopes which use pinhole to reject out of focus light, it is possible to implement a confocal slit in the SPIM setup that rejects out of focus light. If one uses a SPIM setup that creates light sheet by scanning the beam across the focal plane, then using a camera in a rolling shutter mode it is possible to synchronize the active pixels with the light beam. Then only those pixels will be read out where the beam lies, see figure 2.5. In this case part of the out of focus light will be rejected by disabled pixels. With the confocal slit arrangement it is possible to increase the SNR up to two times compared to global shutter mode where all pixels are read out at once [44]. This method is easy to implement with digitally scanned light sheet and increases the SNR without compromising the temporal resolution.

2.5.2 Structured Illumination Method

Another approach to improve SNR in thick biological samples is the structured illumination method (SIM). In the SIM the illumination pattern is alternated using either a grid or a spatial light modulator. To reduce the scattering background at least 3 images ($I_{1,2,3}$), with different illumination patterns have to be captured. If a grid is used then it has to be moved very precisely to at least 3 different positions to create each image [45]. In addition, the sample has to be very stable to make the SIM method to work [46]. To show how the SIM method works let's take as an example three sinusoidal illumination patterns with offset phases 0^o, 120^o and 240^o. Each illumination pattern corresponds to

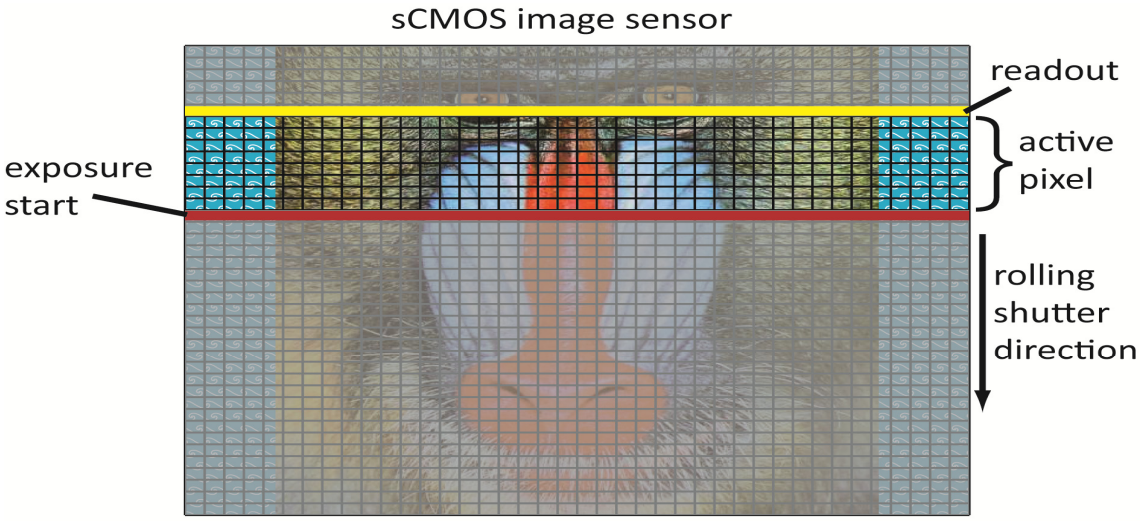

Figure 2.5: Confocal slit arrangement using rolling shutter camera mode [44]

.

an image $I_{1,2,3}$. To enhance the image with SIM one has to use the following equation [47]:

$$I_{SIM} = \sqrt{\frac{(I_1 - I_2)^2 + (I_2 - I_3)^2 + (I_3 - I_1)^2}{2}} \tag{14}$$

Using this simple method it is possible to increase the signal to background ratio up to 7 times [48]. Besides increase in SNR, structured illumination can be used to increase the resolution. The maximum spatial frequency that will be transmitted through the microscope can be calculated via equation

$$k_M = \frac{2NA}{\lambda}, \tag{15}$$

where k_M is the maximum observable spatial frequency, λ is fluorescence wavelength and NA is the numerical aperture of the objective. For an aberration-free microscope, the OTF would look like a disk with a radius k_M. Therefore a microscope acts as a low pass filter, which lets to go through only spatial frequency below k_M. But, if the sample is illuminated with a pattern with known frequency k_{SIM}, then the image can be seen as a sum and difference frequencies of objects spatial frequency k_O and pattern frequency k_{SIM}, see figure, 2.6. Black lines corresponds to the object's spatial frequency, and blue lines represents the structured illumination pattern. As a result pattern with lower spatial frequency is observed, see figure 2.6. Therefore using structured illumination the microscope's maximum observable spatial frequency can be increased to $k_M + k_{SIM}$.

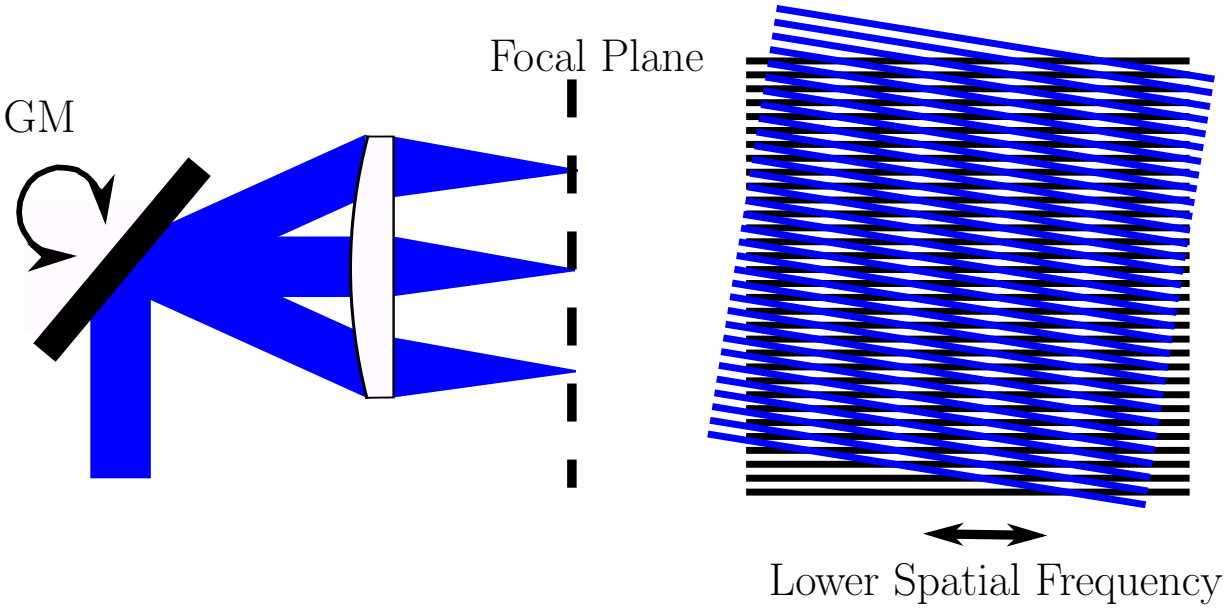

Figure 2.6: Structure Illumination Method. Left: GM - galvo mirror. Right: black lines correspond to object, blue lines correspond to structured illumination pattern.

3 Materials and Methods

3.1 Design of light sheet microscope

3.1.1 Illumination Arm

An aim is to build a microscope that would be able to image large samples, up to 1 cm in diameter, maintaining relatively high resolution in all 3 dimensions. To achieve high axial resolution throughout the whole field of view, the beam has to be thin and with small divergence. Otherwise the resolution at the sides of the image is going to be much worse than in the middle part.

The first step to make a design is to choose the light source for the illumination. In our setup a diode laser with 488nm emission wavelength is used for a light sheet creation (Coherent Obis LS 100mW, 0.8mm output beam diameter). The spectral region of the laser was chosen to match the absorption maximum of fluorescent green protein, which is commonly used fluorophore in modern fluorescence microscopy. To excite fluorophores that emit light in red and infrared regions a diode laser with 640nm emission wavelength is used (Coherent Obis LX 100mW, 0.8mm output beam diameter). These lasers have good Gaussian beam quality which is required for precise light focusing. In addition, a good Gaussian beam profile is needed for high quality Airy beam creation. As we are planing to do multi spectral imaging, all of the light sheet forming optics have to be achromatic.

At first the beams from 640nm and 488nm lasers are combined together using a dichroic mirror. Then the beam enters a variable beam expander (BE) (Edmund optics 2-8x magnification) which is achromatic in the wavelength region between 400-750nm. The beam expander is used to change the width of the beam, as a result the NA of the final focusing lens will change. Therefore using the BE it is possible to change the thickness of the beam at the focal plane. If the sample is illuminated using an Airy beam, then after the BE Airy optics (AO) is included, see figure 3.1.

After the beam expander, the beam is reflected from a rotating galvo mirror (GM). Galvo mirror is an electromechanical device that deflects the incoming beam in a specific angle that is proportional to the applied voltage. The galvo mirror sweeps the beam back and forth to create digitally scanned light sheet. The DSLS gives a homogeneous intensity light sheet. Besides, by synchronizing the galvo mirror with the camera roller shutter mode readout, it is possible to form a confocal slit arrangement. As a result, the

SNR can be increased. Moreover the digitally scanned light sheet allows also structured illumination without additional optics. In this case the laser intensity has to be modulated and synchronized with the galvo mirror.

To make the outgoing beams parallel to each other a scan lens (SL) is used. In our setup the scan lens consists of 2 plano convex achromatic spherical lenses (f=150mm, D=50mm). The first lens is placed at the focal distance from the galvo mirror, and the second lens is placed to make a Plossl eyepiece. The Plossl eyepiece consists of 2 spherical achromatic lenses which are placed closely together. The focal length of the Plossl eyepiece can be calculated as [49]:

$$F = \frac{f_1 \cdot f_2}{f_1 + f_2 + d}, \tag{16}$$

where f_1 is the focal length of the first lens, f_2 is the focal length of the second lens and d is the separation distance of the lenses. This setup makes the output beams less divergent and increases homogeneity compared to single lens [50].

As we are going to image large samples, the light going through them will be attenuated. Therefore one side of the image will be with reduced intensity. To make uniform intensity one has to illuminate the sample from both sides. To have illumination from both sides of the sample a 50:50 beam splitter (BS) is inserted in the beam path. Illumination from both sides gives more even intensity distribution throughout the light sheet. Besides, when Relay optics is used, the imaging speed can be increased by a factor of 2 [51]. The speed improvement can be achieved, because the second beam after relay optics will be on the opposite side of the focal plane. Therefore galvo mirror via scanning two times smaller angle can cover the same field of view.

After the beam splitter, collimation lenses (CL) (spherical achromatic lenses f=150mm, D=50mm) are inserted to collimate the beam for both beam paths. To create the light sheet, focusing lenses (FL) are used (spherical achromatic lens f=100mm, D=50mm). As big samples are going to be imaged, the working distance of the focusing optics has to be bigger than the sample size. This lens has 96mm long working distance. Moreover much wider light sheets can be created with lenses compared to microscope objectives.

3.1.2 Detection arm

The detection arm is used to collect the fluorescent light that comes from the light sheet. Therefore the microscope objective is placed to have the light sheet in the focal plane, see figure 3.2. To image large samples one has to use objectives with big field of view and long working distance (WD). In our setup two different objectives are used. First is Nikon AZ Plan Apo 1x with 3cm working distance and 0.1 numerical aperture. The second objective is Nikon AZ Plan Apo 4x with WD=20mm and NA=0.4. Using Rayleigh diffraction limit one can calculate the theoretical resolution of these objectives:

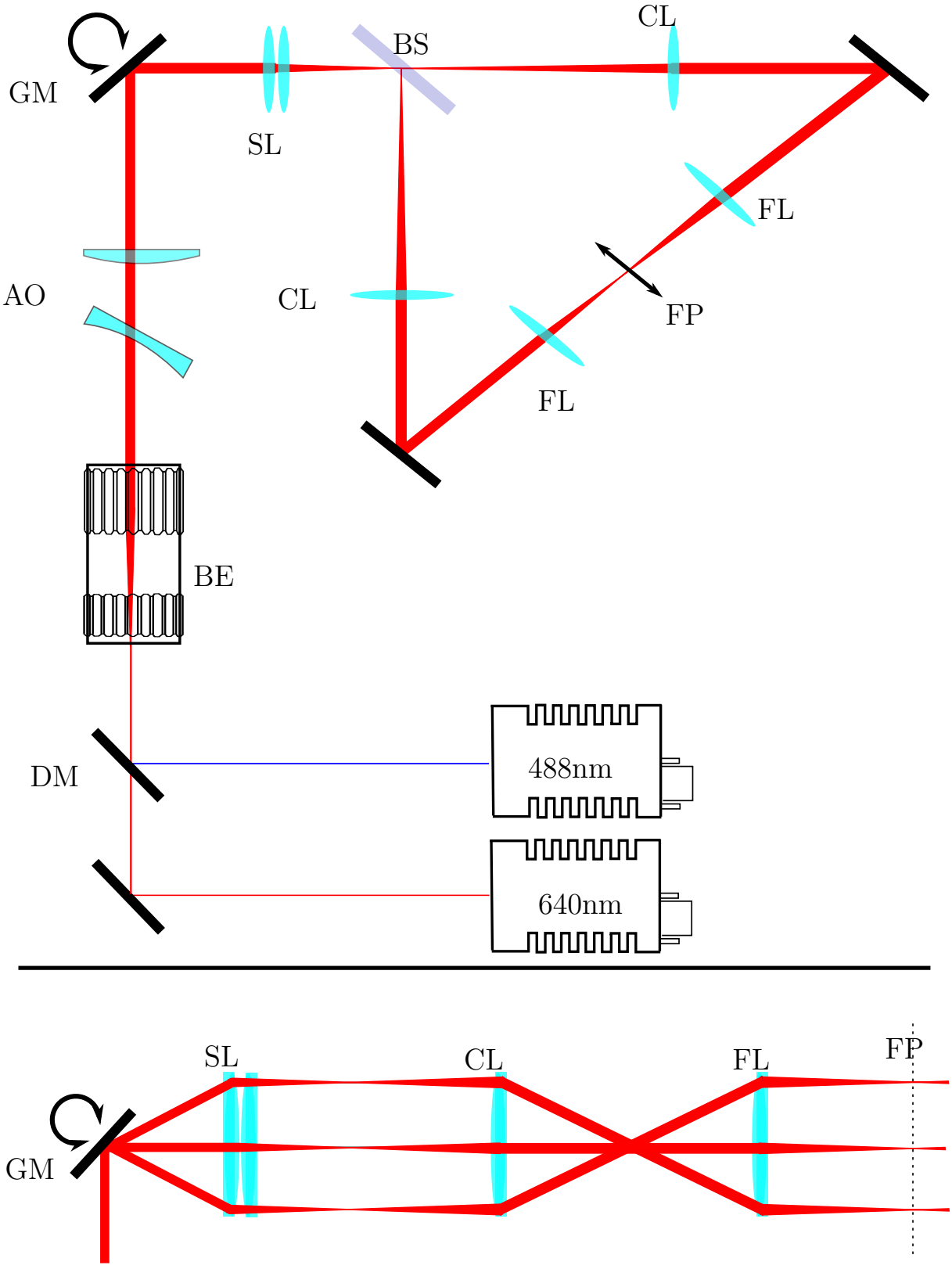

Figure 3.1: Scheme of the light sheet formation setup. DM - dichroic mirror, BE - beam expander, AO - Airy optics, GM - galvo mirror, SL- scan lens, BS - beam splitter, CL - collimation lens, FL - focusing lens, FP - focal plane.

$$d_{x,y} = \frac{1.22\lambda}{2NA} \tag{17}$$

Therefore, the theoretical lateral resolution resolution using 515nm emission fluorescent light from green fluorescent protein is 3.14 μm with 0.1 NA objective and 0.785μm with 0.4NA objective. Besides the lateral resolution we can also calculate the Abbe's axial resolution limit via

$$d_z = \frac{2\lambda}{NA^2}. \tag{18}$$

From this equation it follows that the depth resolution of a 0.1NA objective is 103.0 μm and with 0.4 NA objective d_z is 6.43μm.

Both objectives are infinity corrected, meaning that outgoing light will be collimated. Because the light rays are parallel to each other it is convenient to use an optical filter to filter out scattered excitation light from the fluorescent light, see figure 3.2. After optical filters, (1x-8x magnification) zoom body is placed in. With the zoom unit it is possible to change the resolution and the field of view.

After the zoom body, an achromatic tube lens is placed that focuses the collimated light on the camera and the tube lens demagnifies the image 0.6 times. To record an image a sCMOS camera is used (Andor Zyla 4.2 100fps 4.2 Mpix with pix size 6.5μm, $QE_{max} = 0.82$). To move the sample through the light sheet along the detection axis, a stepper motor (SM) is used with step size resolution of 100nm. Using 0.4NA objective and 8x zoom, the pixel in the image will correspond to approximately 338.5nm and the field of view of this arrangement is 640μm. And with 1x zoom it is possible to achieve 3.385 μm lateral resolution and 6.43μm axial resolution for field of view up to 5.12mm large. The maximum achievable FOV is with 0.1 NA objective and it is 20.5mm with 10.83 μm resolution and 103μm axial resolution. One can see the pixel size and corresponding FOV in the table 3.1.

0.1 NA objective		0.4 NA Objective	
Pix. size, nm	FOV, μm	Pix. size, nm	FOV, μm
1354	2773	338.5	640
1548	3169	387	731
1806	3697	451	853
2167	4437	541	1024
2708	5546	677	1280
3611	7394	903	1707
5415	11092	1354	2560
10830	22184	2708	5120

Table 3.1: Pixel size and field of view with 0.1 and 0.4 NA objectives.

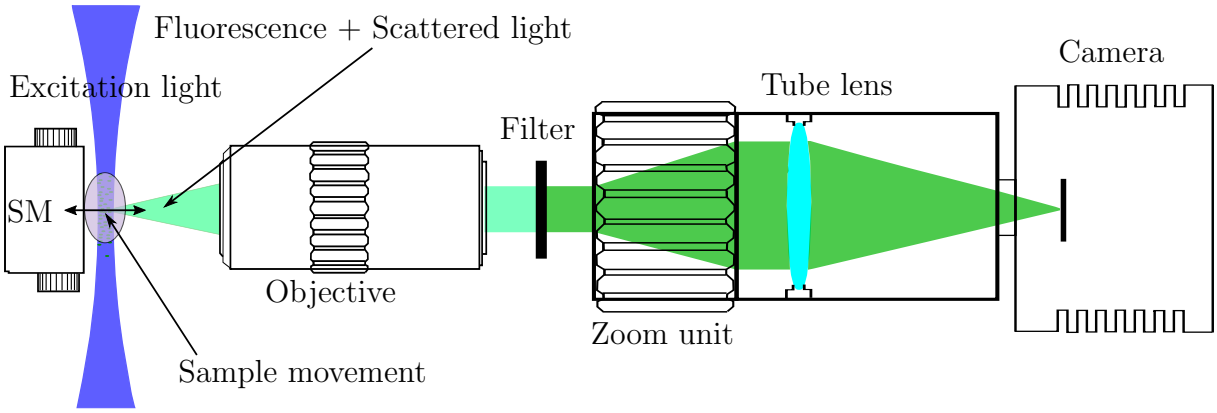

Figure 3.2: Light path through the detection arm. SM - Stepper motor.

3.2 Design of Airy beam forming optics

There exists several techniques how to create Airy beams. In our setup two precisely misaligned cylindrical lenses were used to induce cubic phase modulation on an incoming Gaussian beam. Theoretically two lenses with the same focal length and opposite signs would give the best results. But, if very short focal length lenses are used, then the lenses have to be close together, therefore it is hard to adjust the lenses to create good quality Airy beam. If long focal lens lenses are used, then it is hard to collimate the beam, leading to reduced Airy beam quality. Thorlabs provide 50mm and 70mm focal length cylindrical lenses. To study which focal length lenses would give better quality, Airy beams we used FRED Optical Engineering Software.

The FRED Optical Engineering Software simulates the light propagation through optical elements and optical media taking in to account all the light properties, like interference, diffraction, polarization, e.t.c. FRED optics engineering software uses the tested and proven method of Gaussian beam decomposition for propagating coherent fields through opto-mechanical systems by complex ray tracing [52]. This technique allows for general modelling of coherent fields and makes it possible to simulate laser systems, interferometers, holographic systems, and even some specific applications of partial coherence.

A FRED software script was written to find the optimal lens positions for beam collimation. It was done for different first lens tilt angles in the range from 20-45 degrees. And then using the data for best light collimation an Airy beam was simulated.

3.3 Fluorescent Bead Sample Preparation

To measure the point spread function of the microscope, a fluorescent bead sample is needed. When the point spread function of two dimensional microscopes has to be characterized then the sample preparation is relatively easy. First, fluorescent bead solution has to be diluted in a low concentration, because the beads have to be well separated.

Otherwise, fluorescence light from the neighbouring bead will distort the measurement of PSF. Second, the diluted solution of fluorescent beads has to be pipetted on a sample glass and dried out.

When a 3D PSF has to be measured, then the beads have to be in a three dimensional matrix. To restrict the movement of the beads the matrix has to be solid or liquid with high viscosity. Besides, the matrix has to be with low scattering coefficient and absorption coefficient. Usually as a matrix for fluorescent beads and biological specimen agar gel is used. The agar gel is made from distilled water and agar powder. The mass concentration of agar is from 0.5-2%. At first water and agar powder is mixed together using vortex stir. The agar dissolves in water above 92 °C, therefore the solution is heated in the microwave up to 100 °C. After the boiling point is reached, the solution is again stirred and cooled down to 40 °C. Then the solution is filled in a cuvette and mixed with diluted fluorescent bead solution. Agar solution sets to a firm gel below 35 °C. The Agar gel contains $98 - 99.5\%$ water, therefore it will have almost the same refractive index and absorption coefficient. But the agar gel has considerably larger scattering coefficient. The transparency of agar gel is good enough to image small samples up to few mm big. But for large samples the agar gel is opaque, and the scattered light makes the images blurry.

To reduce the scattering coefficient we used an agar substitute produced from a bacterial fermentation(Sigma Aldrich, Phytagel). The preparation is similar to the agar sample preparation protocol, but in this case $MgSO_4$ salt is added in the first step [53].

4 Results and Discussion

4.1 The resolution and field of view of the Gaussian beam

At first the width and the Rayleigh length of Gaussian beams were measured. First, a quarts cuvette was filled with low concentration fluorescin fluorophore solution. Fluorescin has a high absorption peak near 488nm. The excitation beam was sent through the cuvette and the fluorescence light was imaged with the microscope. In Figure 4.1 one can see the measurement of a Gaussian beam with 6x magnification of beam expander value. To determine the beam width and the laser sheet length, results were fitted with the equation 4. The results agree very well with the theoretical fit. The best axial resolution

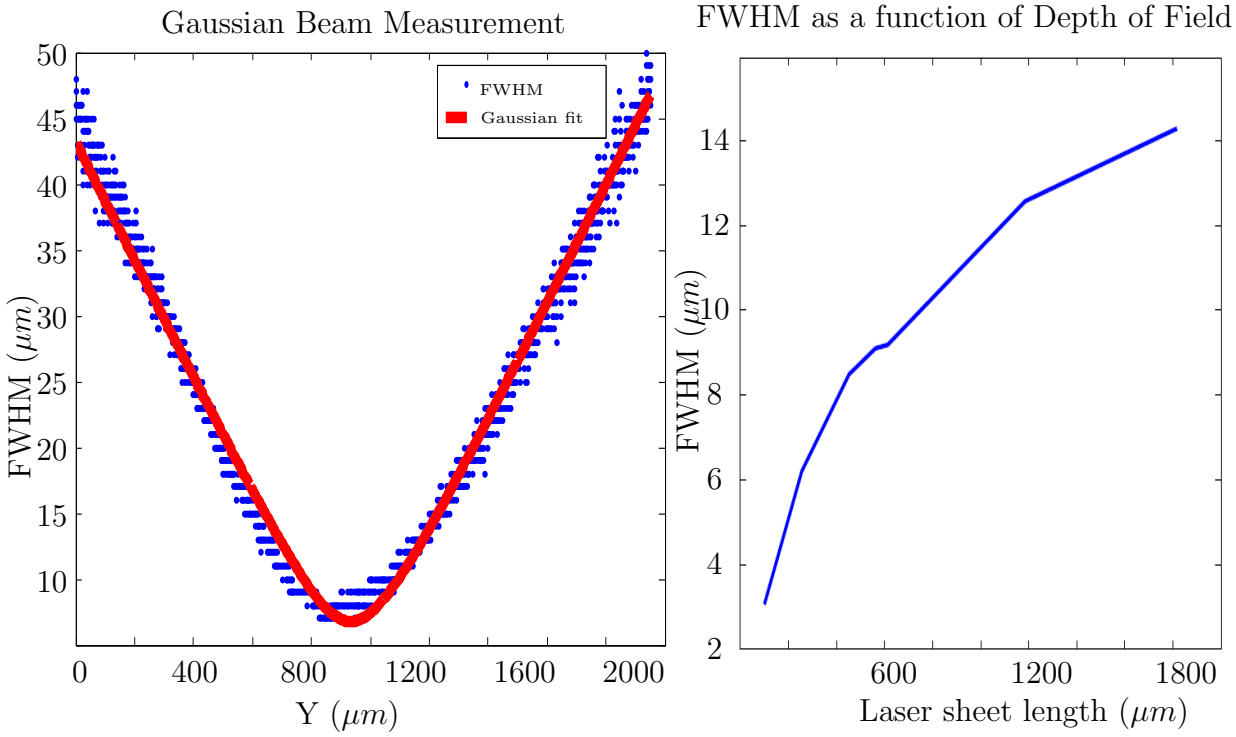

Figure 4.1: Left: Gaussian beam FWHM measurement with 6x beam expander magnification. Right: the measured Gaussian beam FWHM as a function of laser sheet length.

what can be achieved with this system is 3.05 μm, and the FOV corresponding to this

width is $98.5\mu m$. With the smallest beam expander magnification the width of the beam is 14.3 μm and the depth of field is $1821\mu m$

4.1.1 Gaussian Point Spread Function Measurement

To determine the resolution of the microscope in all three dimensions a three dimensional point spread function was measured. Fluorescent beads were imaged to measure three dimensional PSF. At first, local three dimensional intensity maxima were counted. The number of maxima correspond to the bead count. Then, along the brightest pixel, in all three dimensions, a Gaussian function was fitted. In the figure 4.2 one can see a typical image of a bead in all three dimensions. Red line shows the best three dimensional Gaussian fit and blue line is a Gaussian fit along z axis. As one can see the best Gaussian fit is slightly tilted, and on average makes a 2.13° degree angle with the z axis. It means that for better image deconvolution the image stack should be tilted by 2.13 degrees.

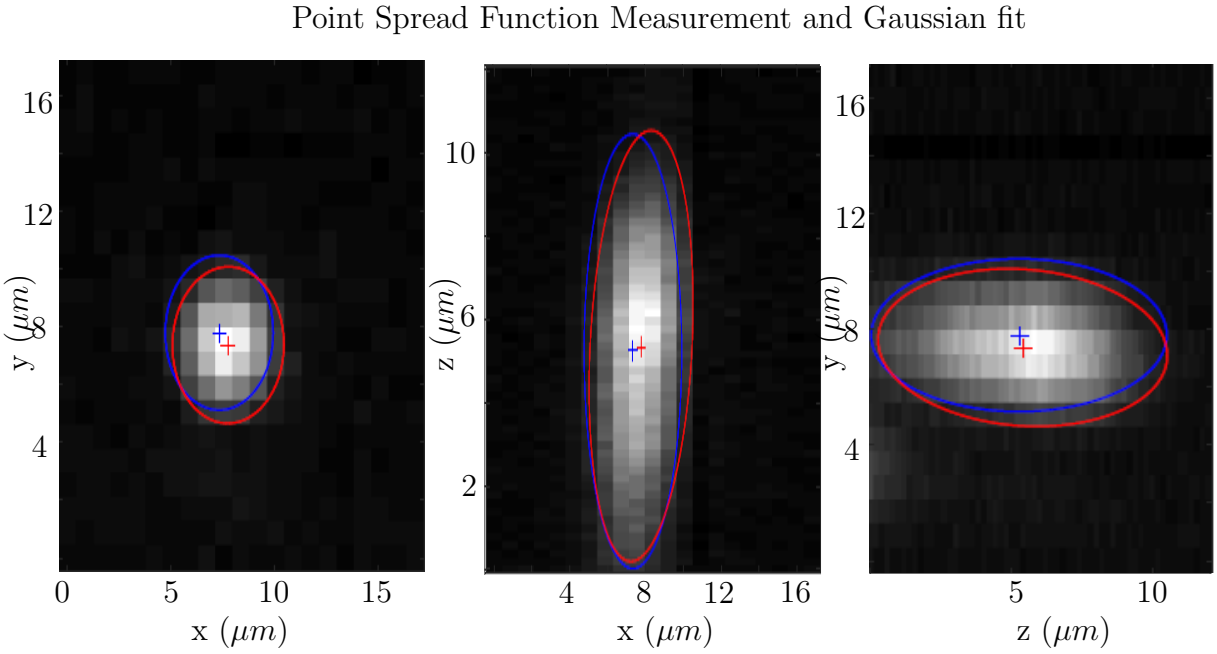

Figure 4.2: Three dimensional point spread function measurement. Red: best Gaussian fit. Blue: Gaussian fit along z axis

Figure 4.3 shows the bead intensity profile for each axis, and the intensity is fitted to a Gaussian function. As one can see, a Gaussian intensity profile fits the measured data very well. Therefore in this arrangement Gaussian PSF can be used for deconvolution.

Typical bead image varies from bead to bead, therefore to determine PSF more accurately a statistical approach was used. Figure 4.4 shows a histogram of 74 bead measurements. The average FWHM along x axis is $2,81\mu m$, along y axis is $2.84\mu m$ and along z axis is $4.34\mu m$. In this measurement excitation beam FWHM is $3.05\mu m$ and the FOV of the imaging system is $1280\mu m$. As the figure 4.1 shows, the depth of field for beam

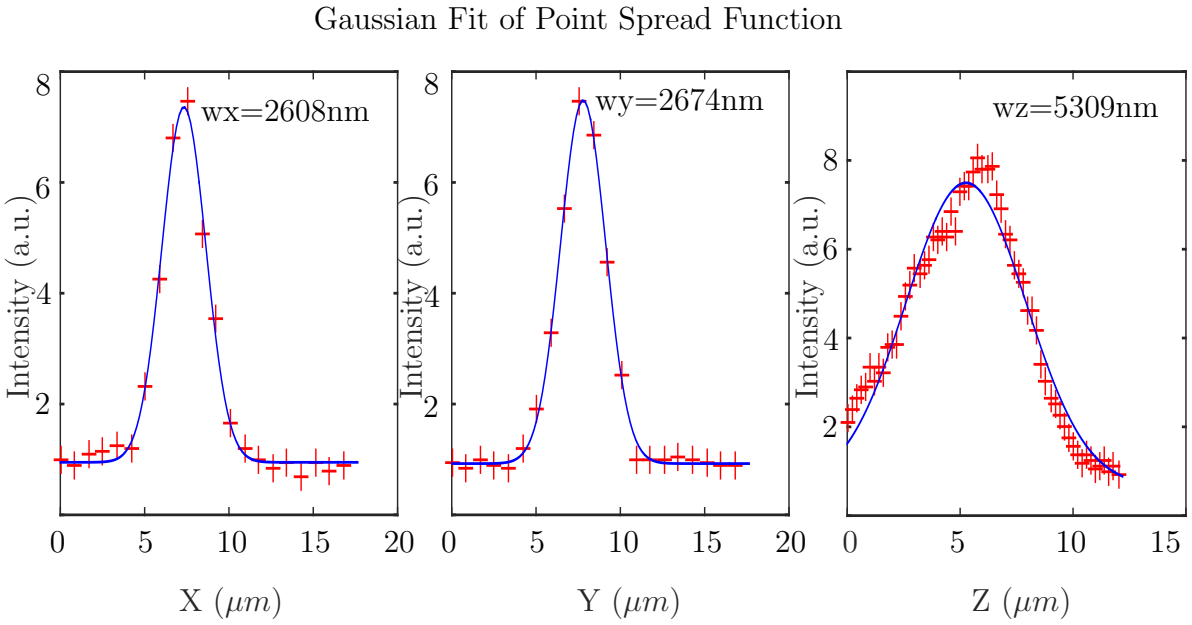

Figure 4.3: Gaussian beam near the focal plane

with 3.05μm FWHM is 98.5μm. Due to the fact that the beam diverges, it is expected that the average bead intensity FWHM along z axis would be much larger than the measured average FWHM. The measured FWHM along z axis is lower than expected because the axial resolution can be seen as multiplication between axial resolution of objective and excitation beam width. In this measurement an objective with 0.4NA was used, and using the equation 18, the axial resolution of this objective is 6.43μm. When 0.4NA objective is used the axial resolution remains in the range of 6μm for FOV of 5.12mm. To extend the FOV objective with 0.1NA is used. In this case the axial resolution of objective is 103μm. And the SPIM microscope average axial resolution for FOV of 1cm is 25.4μm.

4.1.2 Simulations of 1D Airy beam

The Airy beam propagation through two cylindrical lenses and the induced phase modulation was simulated using FRED photonics software. Then the Airy beam profile was measured at the focusing lens focal plane. The simulated Airy beam profile at the focus, for 40° tilt angle of the concave cylindrical lens is shown in the figure 4.5. The coefficient of determination is larger than 99% ($R^2 > 0.99$). The R squared value drops down for smaller than 27° tilt angles, and for larger than 47° concave lens tilt angles. R^2 value is a statistical measure of how close the data are to the fitted regression line. On the right side of the figure 4.5 is plotted for how long distance the FWHM of the first peak remains the same.

The figure 4.6 shows the FWHM of the first peak as a function of propagation

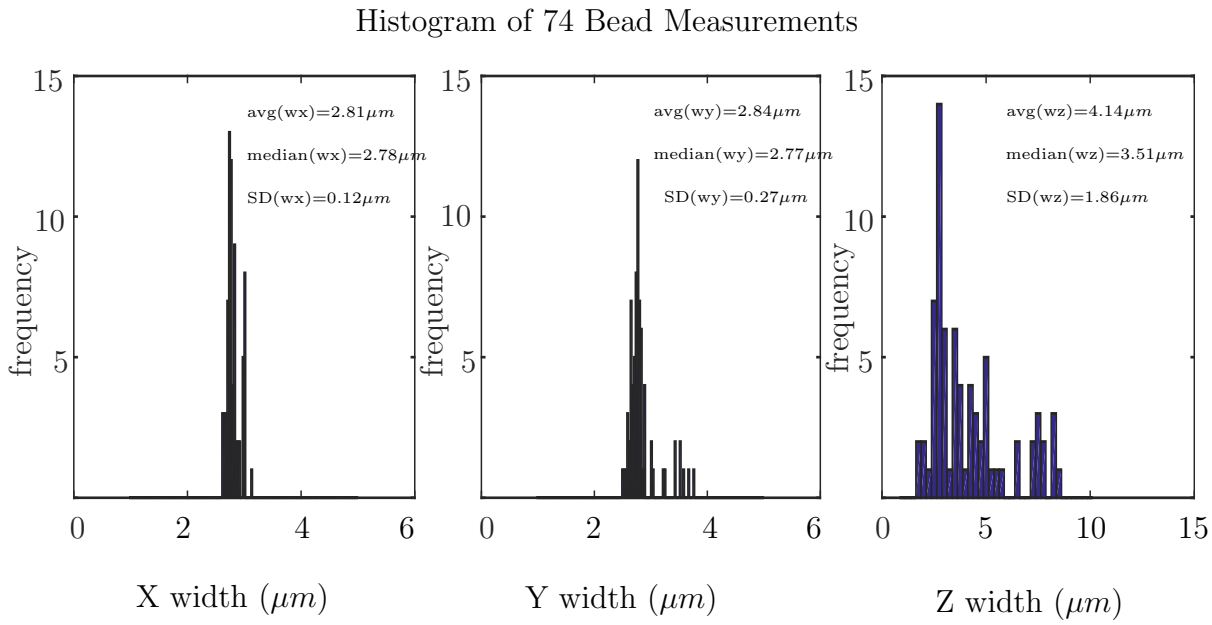

Figure 4.4: Histogram of the point spread function, with measurements from 74 beads.

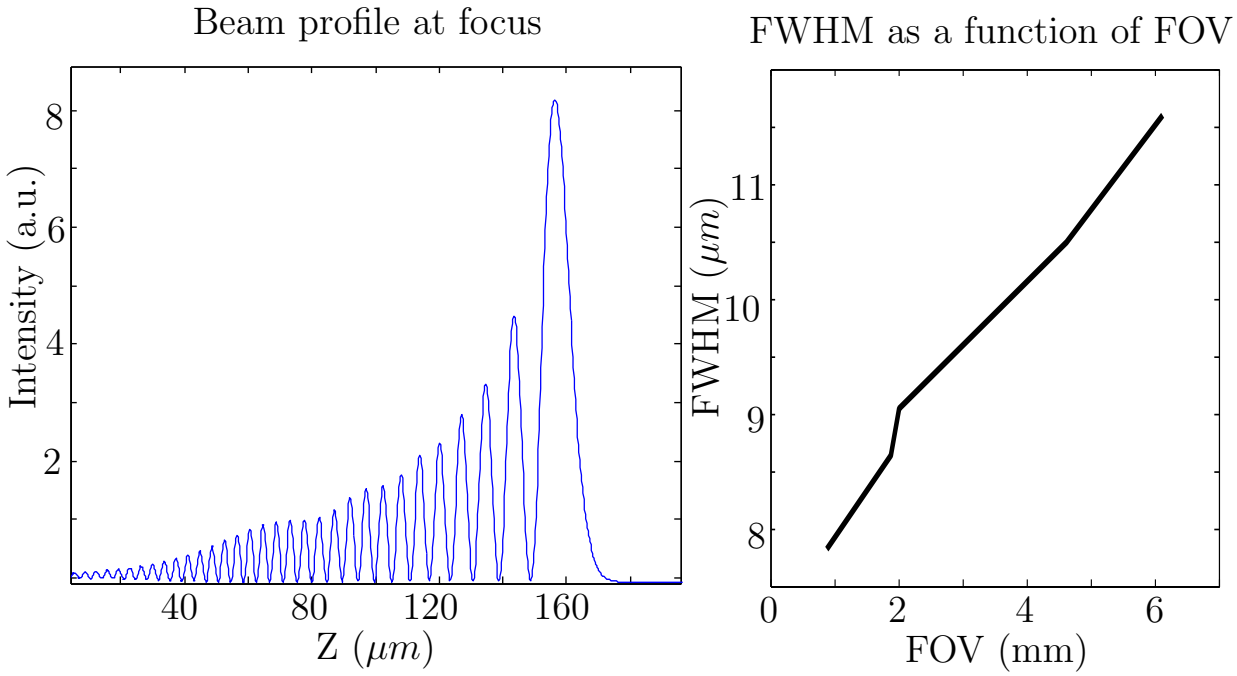

Figure 4.5: 1D Airy beam profile at focal plane

distance near the focal plane for three different concave lens tilt angles. It is evident that the peak width remains close to the minimum value for much longer distances compared to Gaussian beams.

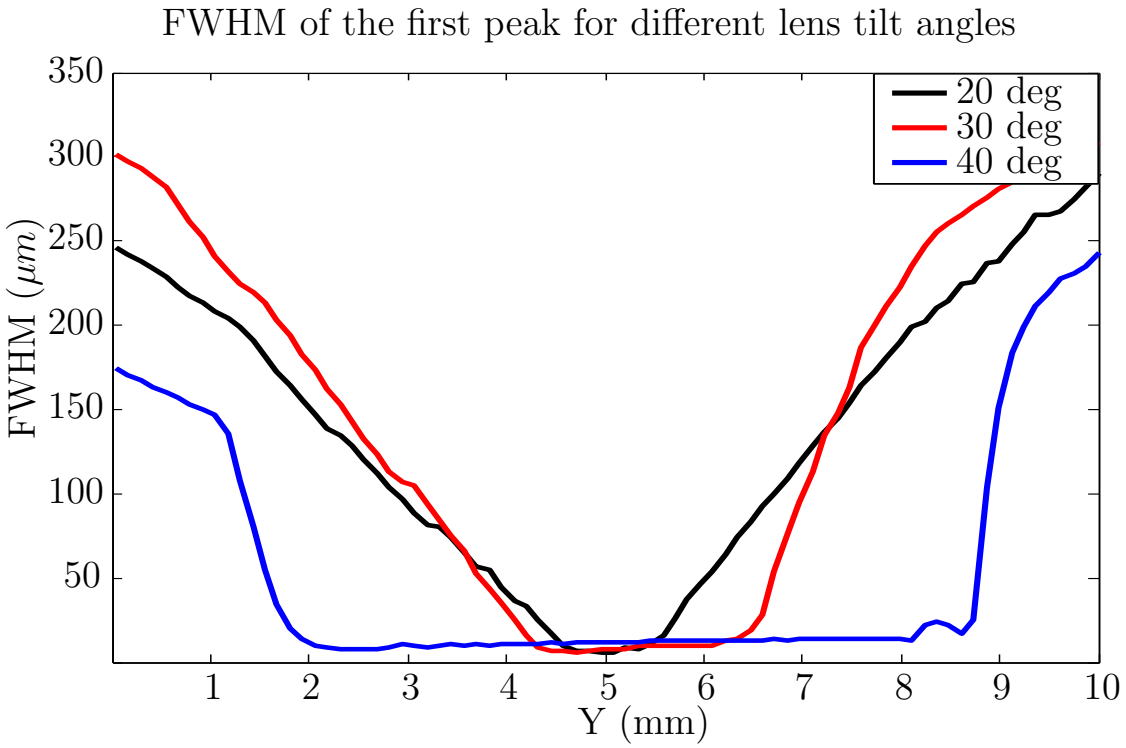

Figure 4.6: FWHM of the first Airy peak along the propagation axis near the focal plane

These simulations shows that it is possible to create high quality Airy beam with two precisely misaligned cylindrical lenses for 25-45 degree tilt angle of the first concave lens.

4.2 Measured resolution and field of view of the Airy beam

The Airy beam profile was measured sending the Airy beam directly on the camera using a mirror in $45°angle$. In the figure 4.7 one can see the beam profile at the focus. It is evident that the measured profile coincides very well with the theoretical fit from equation 7a, and the R squared value is above 99%. From the theoretical fit one can calculate the exponential decay constant a and the constant b, see equation 7b,7c. Then using these constants and using equation 7a one can calculate the beam ballistics along the y and z axis. This data then can be used as a point spread function along z axis for deconvolution.

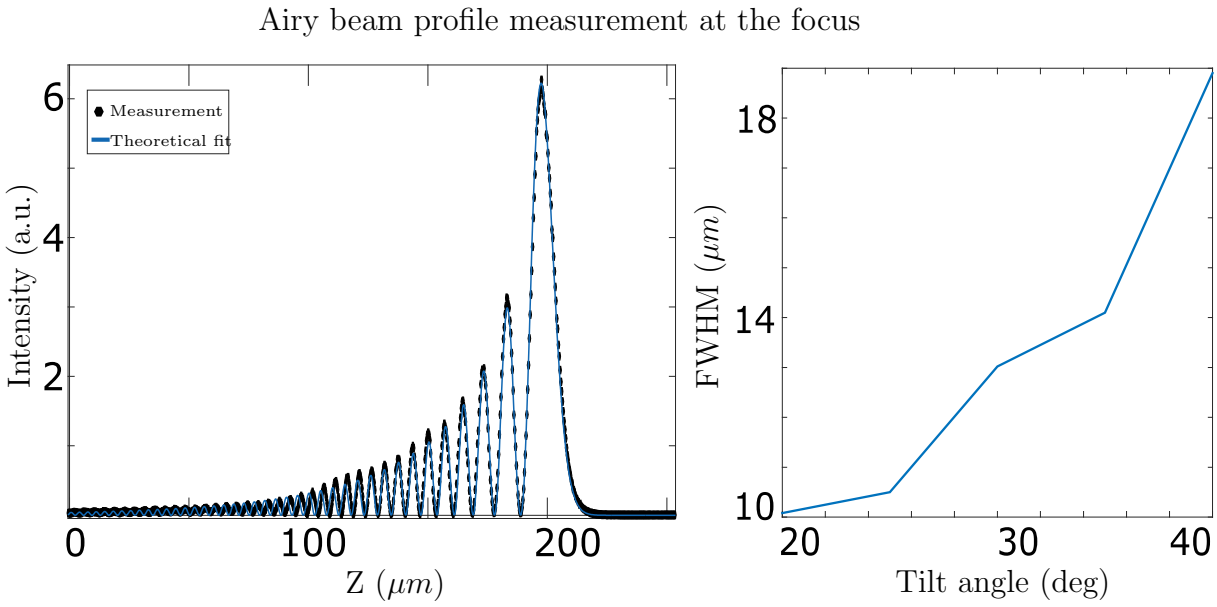

Figure 4.7: Left:Measured Airy beam profile at focus for 30 degree lens tilt angle. Right: FWHM of the first peak as a function of cylindrical concave lens.

4.3 Fluorescent Bead images using an Airy beam

Figure 4.8 shows fluorescent bead image along z and y axis. Using data from the Airy beam profile measurements we deconvolved the image stack, see right part of figure 4.8. In figure 4.9 one can see intensity profile plot along the z axis through the brightest bead pixel. After the Lucy-Richardson deconvolution method, the average bead FWHM along z axis is 7.0μm and the FOV is 5.03mm, with 0.1NA objective. As one can see the deconvolution can not perfectly compensate the axial blur from the Airy beam. Also the bead axial profile does not agree with the theoretical fit as well as the directly measured Airy beam. From the bead profile plot one can see that the minimums of the bead profile does not go to background value. A first reason for the bead profile and measured Airy beam profile difference is that the optical table is not completely isolated from vibrations. Therefore the bead could move along z axis during the exposure, leading to less distinct peaks and minimums. Besides the vibrations, the bead sample is slightly scattering medium, therefore leading to less distinct peaks and minimums of the Airy profile.

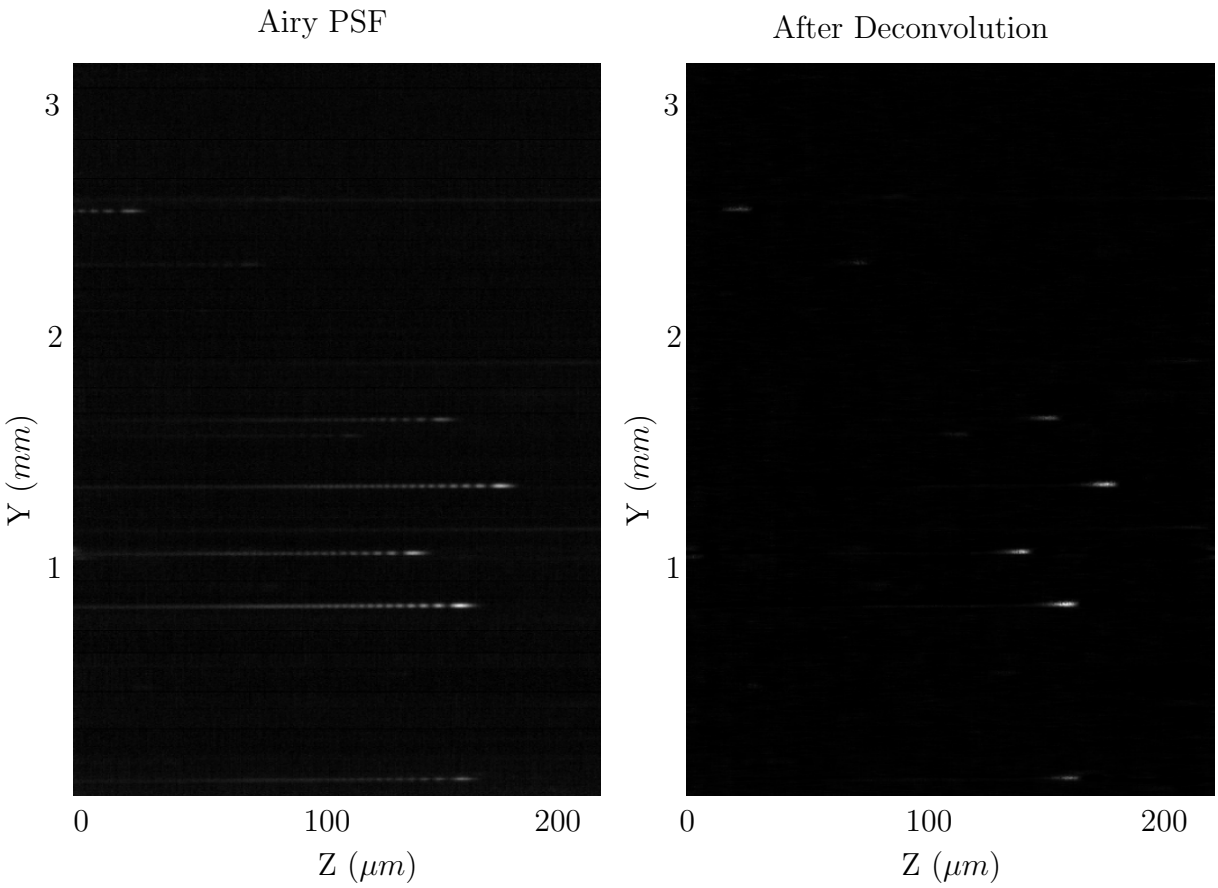

Figure 4.8: Measured Point spread function along z axis using an Airy beam. On the right: deconvolved beads image.

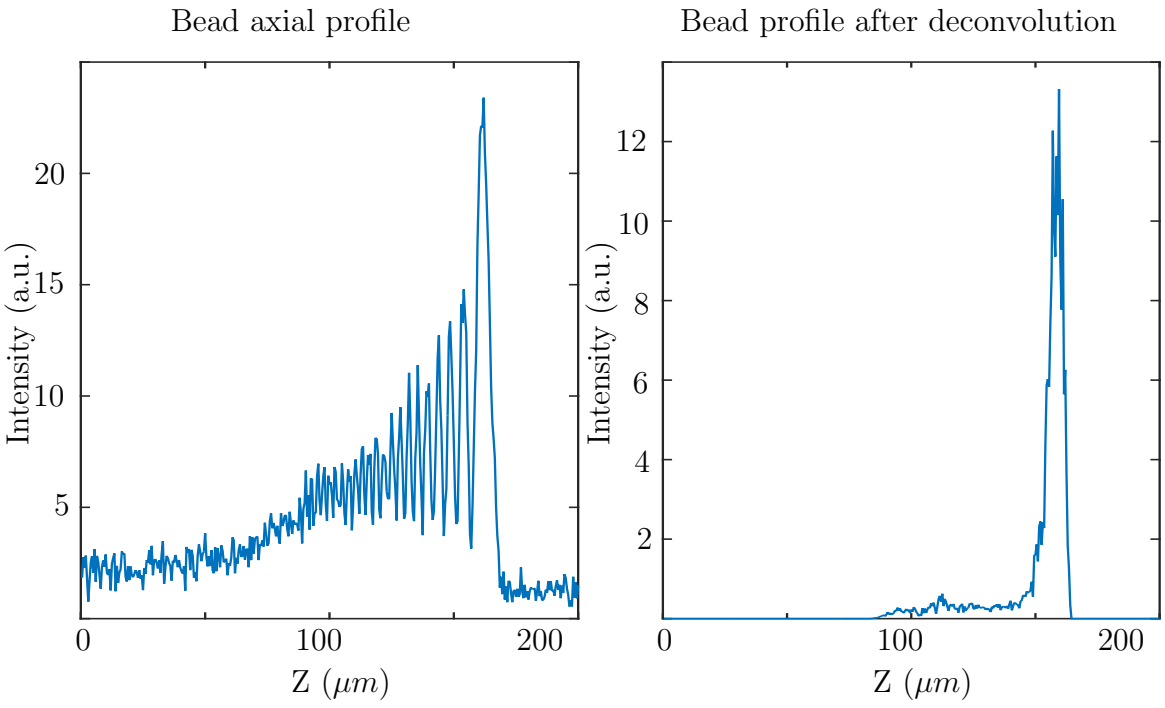

Figure 4.9: Bead profile along z axis before and after deconvolution

4.4 Airy beam and Gaussian beam comparison

Fluorescent beads were imaged using Airy beam and Gaussian beam with two objectives (0.1NA and 0.4NA). In the table 4.1 one can see the measurement results. Using 0.1NA objective in terms of axial resolution the Airy beam outperforms Gaussian beams. This is true when big field of view is needed. with Airy beams it is possible to extend the FOV for approximately 10 times.

When 0.4 NA objective was used then the axial resolution remains nearly the same for FOV 1240-5120 μm. This is due to the fact that the axial resolution can be seen as a multiplication between objective axial resolution and the excitation light beam width. The theoretical axial resolution of the 0.4NA objective is 6.43 μm therefore for FOV that are bigger than 1 mm the resolution will be determined by the objective axial resolution. To increase the axial, resolution the focusing lenses have to be replaced by objectives in order to create very thin light sheets. With current optics the Airy beam does not give any advantage when it is used with 0.4 NA objective, because the OTF of the 0.4NA objective allows higher spatial frequencies, than the Airy beam has. To achieve higher axial resolution than the 0.4NA objective has, the excitation light focusing lens has to be changed with microscope objective.

Gaussian beam 0.1NA		Airy beam 0.1NA		Gaussian beam 0.4NA	
Axial res., μm	FOV, μm	Axial res., μm	FOV, μm	Axial res., μm	FOV, μm
3.2	100	7.0	5200	4.37	640
6.2	500	9.2	8216	7.06	1280
8.6	1000	10.7	11201	7.95	2560
24.3	5000	14.1	19611	7.84	5120
32.1	10000				
36.5	20000				

Table 4.1: Axial resolution and Field of view for Gaussian and Airy beams with 0.1Na and 0.4 NA objectives.

5 Conclusions and Outlook

The first aim of this thesis was to design a selective plane illumination microscope for large sample imaging up to few mm in diameter. The design allows selective plane illumination as well as epi-illumination microscopy. The optical components are arranged to make the light sheet as homogeneous as possible throughout the field of view.

As the samples usually are stained with multiple fluorophores, the SPIM setup had to be designed to allow multispectral imaging. Therefore achromatic lenses were proposed for beam collimation and focusing. The first intent of this microscope is to image large samples. Light going through a big specimen inevitably is going to be scattered. The scattered light excites the fluorophores outside the focal plane of detection objective, therefore reducing the signal to noise ratio. The optical design was made to allow two different approaches to increase SNR without introducing any additional optics in the beam path. The first method is beam synchronization with rolling shutter camera readout mode, making confocal slit arrangement. The second technique is to implement structured illumination pattern by modulating the laser output power. Moreover, with SIM method it is possible to increase the microscope's lateral resolution.

The next step of the project was to study if high quality Airy beams can be created using two precisely misaligned cylindrical lenses. To do so we used FRED photonics software to simulate the light propagation through the two lens system and beam focusing optics. The simulations showed that high quality Airy beams can be created using 2 cylindrical lenses. The coefficient of determination for these simulations is above 0.99 (R^2 ¿ 99%) when compared to theoretical Airy beam. From the FRED simulations followed that by introducing 2 cylindrical lenses in the beam path it is possible to create an Airy beam in the focal plane of the focusing lens.

The third aim was to built the designed SPIM microscope. The light sheet formation optics were built around Nikon microscope with two different objectives.

The results show that using the constructed SPIM microscope we can create high quality Gaussian light sheets. The maximum resolution using Gaussian beams is $3.05\mu m$ with $98.5\mu m$ FOV. The measured axial resolution using 0.4NA remains almost the same and is determined by the objective axial resolution. Therefore it is possible to achieve $7.8\mu m$ axial resolution for field of view up to 5.12mm. When a 0.4NA objective is used, the SPIM arrangement with a Gaussian beam does not improve the axial resolution. The exception is when very small field of view is used. When 0.1 NA objective is used then

the axial resolution is considerably improved using side illumination with Gaussian beam.

After the Gaussian beam measurements, the optical system was adapted with Airy beam forming optics. The measured Airy beam coincides very well with theoretical function. In the range of 25-45 degree first concave lens tilt angles the R^2 value was above 99% compared to theoretical Airy profile at the focus. It means that outside this tilt angle range the telescopic arrangement cannot compensate other aberration therms, therefore in the focal plane the Airy pattern is washed out. In the range of 25-45 degree tilt angle the cubic aberrations are significantly stronger than the first, second and higher order aberrations. The measurements of fluorescent beads using Airy beams show that the axial resolution is significantly better compared to Gaussian beams when big fields of view are needed.

For image enhancement different algorithms were used. The best results for bead image enhancement gave RichardsonLucy deconvolution algorithm. The disadvantage of this deconvolution method is that it is an iterative algorithm, therefore it requires high computing power and long period of time for large image stack deconvolution. It took approximately 5 minutes for relatively simple single bead image deconvolution. For that reason to deconvolve large image stacks Wiener deconvolution filter should be used. The disadvantage of Wiener deconvolution method is that it gives negative pixel values and the deconvolved image is more blurry compared to deconvolved image with Lucy-Richardson method. The blind deconvolution algorithm can not be used for image enhancement when Airy beams are used, because the Airy PSF is not an analytical function and in our setup it spans for 100 μm. Therefore the blind deconvolution algorithm requires very long time periods for deconvolution even for simple bead image deconvolution.

The deconvolution outcome can be improved if Airy beams with higher exponential decay parameter are used. Higher exponential decay constant leads to less peaks. besides the first peak becomes more distinct from other Airy peaks. To increase the decay parameter lenses or objectives with higher NA have to be used for light sheet formation.

The measured axial resolution of Gaussian and Airy beams shows that the maximum resolution can be achieved with Gaussian beams, but the FOV is restricted to $100\mu m$. For instance with the current setup using Gaussian beams the maximum resolution is $3\mu m$ and with Airy beams $7\mu m$. The corresponding FOV is $100\mu m$ for Gaussian beam and $5120\mu m$ for Airy beam. Using Airy beam it is possible to increase the FOV approximately eight times compared to Gaussian beams. These results show that using an Airy beam it is possible to significantly increase the FOV maintaining high axial resolution. A human cell on average is around 20 micrometer in the diameter [54]. Therefore using Airy beams it is possible to make a wide field microscope that would have single cell resolution in all 3 dimensions for fields of view up to 1 cm. This is an important advancement since Airy beams would allow larger sized objects, e.g. optically cleared tissue specimens, to be imaged with high resolution.

Unfortunately the software that we use to control the Nikon microscope stepper motor and sCMOS camera does not sustain light sheet mode, therefore it is not possible to control the galvo mirror with the Nikon Elements software. To implement the confocal slit arrangement and structured illumination method we have to make custom made software based on the National Instruments LabView software. The next steps of this project are summarized in the following bullet list.

- Create confocal slit arrangement by synchronizing the galvo mirror and roller shutter mode camera readout.
- Implement structured illumination method
- Image optically cleared tumors
- Change the focusing lenses to objectives and image single cells

Bibliography

[1] "The nobel prize in chemistry 2014 - press release," http://www.nobelprize.org/nobel_prizes/chemistry/laureates/2014/press.html, accessed May 5, 2016.

[2] S. Svanberg, *Atomic and molecular spectroscopy: basic aspects and practical applications*, Vol. 6 (Springer Science & Business Media, 2012).

[3] W. Demtröder, *Atoms, Molecules, and Photons* (Springer, 2006).

[4] B. Valeur and M. N. Berberan-Santos, *Molecular fluorescence: principles and applications* (John Wiley & Sons, 2012).

[5] J. R. Lakowicz, *Principles of fluorescence spectroscopy* (Springer Science & Business Media, 2013).

[6] A. Nasevicius and S. C. Ekker, Nature genetics **26**, 216 (2000).

[7] T. Yoshimizu, N. Sugiyama, M. De Felice, Y. I. Yeom, K. Ohbo, K. Masuko, M. Obinata, K. Abe, H. R. Schöler, and Y. Matsui, Development, growth & differentiation **41**, 675 (1999).

[8] K. Greger, J. Swoger, and E. Stelzer, Review of Scientific Instruments **78**, 023705 (2007).

[9] P. Davidovits and M. Egger, Applied Optics **10**, 1615 (1971).

[10] A. Diaspro, Confocal and Two-Photon Microscopy: Foundations, Applications and Advances, by Alberto Diaspro (Editor), pp. 576. ISBN 0-471-40920-0. Wiley-VCH, November 2001. , 576 (2001).

[11] H. Siedentopf and R. Zsigmondy, Annalen der Physik **315**, 1 (1902).

[12] B. R. Masters, eLS (2010).

[13] H. Siedentopf and R. Zsigmondy, Ann Phys **10**, 1 (1903).

[14] "The nobel prize in chemistry 1925," http://www.nobelprize.org/nobel_prizes/chemistry/laureates/1925/, accessed May 5, 2016.

[15] J. Huisken and D. Y. Stainier, Development **136**, 1963 (2009).

[16] E. G. Reynaud, J. Peychl, J. Huisken, and P. Tomancak, Nature methods **12**, 30 (2015).

[17] L. Gao, L. Shao, B.-C. Chen, and E. Betzig, Nat. Protoc **9**, 1083 (2014).

[18] L. Gao, Biomedical optics express **6**, 881 (2015).

[19] A. Muto, M. Ohkura, G. Abe, J. Nakai, and K. Kawakami, Current Biology **23**, 307 (2013).

[20] M. Mickoleit, B. Schmid, M. Weber, F. O. Fahrbach, S. Hombach, S. Reischauer, and J. Huisken, nature methods **11**, 919 (2014).

[21] H.-U. Dodt, U. Leischner, A. Schierloh, N. Jährling, C. P. Mauch, K. Deininger, J. M. Deussing, M. Eder, W. Zieglgänsberger, and K. Becker, Nature methods **4**, 331 (2007).

[22] K. Becker, N. Jährling, E. Kramer, F. Schnorrer, and H.-U. Dodt, Journal of biophotonics **1**, 36 (2008).

[23] S. Saghafi, K. Becker, N. Jährling, M. Richter, E. R. Kramer, and H.-U. Dodt, Journal of biophotonics **3**, 686 (2010).

[24] M. B. N. Balazs, Am. J. Phys **4**, 264 (1979).

[25] G. Siviloglou, J. Broky, A. Dogariu, and D. Christodoulides, Physical Review Letters **99**, 213901 (2007).

[26] D. Papazoglou, S. Suntsov, D. Abdollahpour, and S. Tzortzakis, Physical Review A **81**, 061807 (2010).

[27] T. Vettenburg, H. I. Dalgarno, J. Nylk, C. Coll-Lladó, D. E. Ferrier, T. Čižmár, F. J. Gunn-Moore, and K. Dholakia, Nature methods **11**, 541 (2014).

[28] B. E. Saleh, M. C. Teich, and B. E. Saleh, *Fundamentals of photonics*, Vol. 22 (Wiley New York, 1991) pp. 76–92.

[29] P. J. Keller, A. D. Schmidt, J. Wittbrodt, and E. H. Stelzer, science **322**, 1065 (2008).

[30] P. J. Keller, A. D. Schmidt, A. Santella, K. Khairy, Z. Bao, J. Wittbrodt, and E. H. Stelzer, Nature methods **7**, 637 (2010).

[31] F. O. Fahrbach, V. Gurchenkov, K. Alessandri, P. Nassoy, and A. Rohrbach, Optics express **21**, 13824 (2013).

[32] R. Candelier, T. Panier, S. Romano, R. Olive, T. Pietri, G. Sumbre, and G. Debrégeas, BMC Neuroscience **14**, P97 (2013).

[33] J. Durnin, J. Miceli Jr, and J. Eberly, Physical Review Letters **58**, 1499 (1987).

[34] D. McGloin and K. Dholakia, Contemporary Physics **46**, 15 (2005).

[35] M. Zhao, H. Zhang, Y. Li, A. Ashok, R. Liang, W. Zhou, and L. Peng, Biomedical optics express **5**, 1296 (2014).

[36] J. Wang, J. Bu, M. Wang, Y. Yang, and X. Yuan, Applied optics **50**, 6627 (2011).

[37] P. Acebal, L. Carretero, S. Blaya, and A. Murciano, Photonics Journal, IEEE **4**, 1273 (2012).

[38] M. Born and E. Wolf, *Principles of optics: electromagnetic theory of propagation, interference and diffraction of light* (Cambridge university press, 1999) pp. 149–151.

[39] A. Small and S. Stahlheber, Nature methods **11**, 267 (2014).

[40] B. Huang, W. Wang, M. Bates, and X. Zhuang, Science **319**, 810 (2008).

[41] M. B. Cannell, A. McMorland, and C. Soeller, in *Handbook of biological confocal microscopy* (Springer, 2006) pp. 488–500.

[42] J. W. Goodman, *Introduction to Fourier optics* (Roberts and Company Publishers, 2005).

[43] T. F. Chan and C.-K. Wong, Image Processing, IEEE Transactions on **7**, 370 (1998).

[44] E. Baumgart and U. Kubitscheck, Optics express **20**, 21805 (2012).

[45] T. Breuninger, K. Greger, and E. H. Stelzer, Optics letters **32**, 1938 (2007).

[46] J. Mertz, Nature methods **8**, 811 (2011).

[47] M. Neil, R. Juškaitis, and T. Wilson, Optics letters **22**, 1905 (1997).

[48] A. Mazhar, D. J. Cuccia, S. Gioux, A. J. Durkin, J. V. Frangioni, and B. J. Tromberg, Journal of biomedical optics **15**, 010506 (2010).

[49] G. Saxby, *The science of imaging* (CRC Press, 2010).

[50] A. Negrean and H. D. Mansvelder, Biomedical optics express **5**, 1588 (2014).

[51] Z. Yang, L. Mei, F. Xia, Q. Luo, L. Fu, and H. Gong, Biomedical Optics Express **6**, 1797 (2015).

[52] "Fred photonics software overview," `http://photonengr.com/software/`, accessed May 5, 2016.

[53] J. Langowski, "Biophysics of macromolecules," `http://www.dkfz.de/Macromol/quickfit/beadscan.html`, accessed May 5, 2016.

[54] R. A. Freitas, *Nanomedicine, volume I: basic capabilities* (Landes Bioscience Georgetown, TX, 1999).

Acknowledgments

First of all I want to thank my supervisor Johan Axelsson for giving me the opportunity to work with this very exciting project. When I was struggling Johan was always there with an advice that helped me to overcome the obstacles that hindered my progress. For that I am very grateful. I want also to thank Johan for trusting me and let me work and solve most of the problems independently. Therefore during this master thesis project I have acquired priceless experience for my future career in the field of research.

I want to thank also to my co-supervisor Stefan Andersson-Engels for the advice throughout the master project and also for the help in my future career. Stefan has made such a welcoming environment in the Bio-photonics group, therefore I enjoyed every day that I spent at the university.

I want to thank to my colleagues for the friendly environment. I always appreciated the entertaining conversations during the lunch times and coffee brakes.

Most of all I want to thank my family for the support throughout my studies. You were always there when I needed. You cheered me up in gloomy days when things did not go so well for me. With Your support I could stay focused and do my best throughout the studies.